A hematopoietic stem cell subset that retains memory of prior inflammatory stress accumulates in aging and clonal hematopoiesis

Andy G.X. Zeng[1,2]*, Murtaza S. Nagree[1]*, Niels Asger Jakobsen[3-5,]*, Sayyam Shah[1,] Alexander Murison[1], Jin-Gyu Cheong[6-7], Isabel Lim[1], Liqing Jin[1], Alicia G. Aguilar-Navarro[1,8], Joana Araújo[1,9-12], Darrien Parris[1], Jessica McLeod[1], Hyerin Kim[1], Hoseok Lee[1], Lin Zhang[14,15,16], Mason Boulanger[1], Elvin Wagenblast[1,13], Eugenia Flores-Figueroa[1,8], Bo Wang[14,15,16,17,18], Gregory W. Schwartz[1,18], Steven Z. Josefowicz[6-7], Paresh Vyas[3-5§], John E. Dick[1,2§], and Stephanie Z. Xie[1§]

[1]Princess Margaret Cancer Centre, University Health Network, Toronto, ON, Canada
[2]Department of Molecular Genetics, University of Toronto, Toronto, ON, Canada
[3]MRC Molecular Haematology Unit, MRC Weatherall Institute of Molecular Medicine, University of Oxford, Oxford, United Kingdom
[4]Department of Clinical Haematology, Oxford University Hospitals NHS Foundation Trust, Oxford, United Kingdom
[5]Oxford Centre for Haematology, NIHR Oxford Biomedical Research Centre, Oxford, United Kingdom
[6]Laboratory of Epigenetics and Immunity, Department of Pathology and Laboratory Medicine, Weill Cornell Medicine, New York, NY, 10065, USA.
[7]Immunology and Microbial Pathogenesis Program, Weill Cornell Graduate School, New York, NY, 10065, USA.
[8]Unidad de Investigación Médica en Enfermedades Oncológicas, Centro Médico Nacional Siglo XXI, Instituto Mexicano del Seguro Social, Mexico City, Mexico
[9]Department of Hematology, Centro Hospitalar Universitário de São João, Porto, 4200-319, Portugal.
[10]Faculty of Medicine, University of Porto, Porto, 4200-319, Portugal.
[11]Instituto de Investigação e Inovação em Saúde, University of Porto, Porto, 4200-135, Portugal.
[12]Instituto Nacional de Investigação Biomédica, University of Porto, Porto, 4200-135, Portugal.
[13]Icahn School of Medicine at Mount Sinai, New York, USA
[14]Peter Munk Cardiac Centre, University Health Network, Toronto, ON, Canada
[15]Department of Computer Science, University of Toronto, Toronto, ON, Canada
[16]Vector Institute, Toronto, ON, Canada
[17]Department of Laboratory Medicine and Pathobiology, University of Toronto, Toronto, ON, Canada
[18]Department of Medical Biophysics, University of Toronto, Toronto, ON, Canada

*These authors contributed equally

[§]Co-senior authors: Paresh Vyas, John E. Dick and Stephanie Z. Xie

Lead contact: Stephanie Z. Xie

Abstract

Hematopoietic stem cells (HSC) must persist through a lifetime of infections to ensure life-long blood production, but whether molecular adaptations following inflammatory stress recovery in HSC are linked to aging and clonal hematopoiesis (CH) are unclear. Here, we performed single cell (sc) Multiomics on human HSC isolated from a xenograft inflammation-recovery model. Two transcriptionally and epigenetically distinct HSC subsets expressing canonical HSC programs were identified. Only one showed scATACseq and scRNAseq changes after recovery from TNFα or lipopolysaccharide treatment. This inflammatory memory HSC (HSC-iM) program is enriched in memory T cells and HSC from recovered COVID-19 patients. Importantly, HSC-iM accumulates with age and with CH. Overall, a human HSC subset that retains memory of prior inflammatory stress has implications towards HSC fitness and leukemia transformation.

Introduction

Humans have an enormous demand (~10^{11} cells daily) for hematopoietic output (*1*). Meeting this need over a lifetime is achieved by a complex hierarchy with a pool of dormant long-term hematopoietic stem cells (LT-HSC) residing at the apex, that are distinguished by their self-renewal properties from their immediate downstream progeny, together collectively termed hematopoietic stem and progenitor cells (HSPC) (*2*). Mature blood cells with a finite life span are continuously replenished by bone marrow (BM) HSPC producing three million cells per second in human adults, in a tightly controlled process (*3*). The coordination of daily hematopoietic output with the maintenance of HSC pools over the lifetime of an individual is not well understood, especially in the context of stresses like repeated infections. Transitions between quiescence and activation are essential for human LT-HSC identity and function (*4–8*). Yet, such transitions become dysregulated in human HSC with aging and inflammatory stress (*9–11*).

Adult humans are estimated to have up to 200,000 HSC contributing to hematopoiesis at any one time (*12*). However, HSC also show functional decline after age 65 (*13–18*), with a marked decrease in HSC clonal diversity (*19*) and increased risks for clonal hematopoiesis (CH) (*20*) and blood cancers (*21*). Single cell (sc) transcriptome and epigenome studies have described the HSPC landscape as a continuum (*2*). We had previously identified transcriptional, epigenetic, and functional heterogeneity in LT-HSC where inflammatory pathways represented one of the most prominent sources of such heterogeneity (*4–7*, *22*, *23*). Moreover, the molecular programs responsible for regulating LT-HSC transition from quiescence to activation are linked to inflammatory responses.

Inflammation and the dysregulation of molecular programs regulating inflammation response are connected to the initiation and progression of myeloid neoplasms (*21*, *24*). Genetic predisposition for clonal outgrowths of CH mutations and the discovery of somatic driver mutations for MPN can arise *in utero* (*25–28*). Mouse models have shown that acute inflammation activates HSC, skews them towards myeloid differentiation, and impairs their self-renewal (*29–31*). Conversely, chronic inflammation promotes sustained epigenetic changes (*32*) and accelerates aging in murine HSC (*24*, *33*). Inflammation and aging cause clonal expansion of CH-associated mutations of *Dnmt3a* and *Tet2* in mice (*34–38*). Moreover, some inflammatory response programs such as TNFα via NFkB regulate HSC survival (*22*, *31*). Together, these data imply inflammatory insults could elicit disparate responses in a heterogeneous HSC pool to initiate a preleukemia setting (*39–41*). However, we have a poor understanding of the molecular response programs of human HSC following inflammatory challenge *in vivo,* and whether these responses are relevant to human health and longevity.

Here, we link HSC heterogeneity to COVID-19 infection, aging and CH by interrogating transcriptomic and epigenetic signatures derived from an *in vivo* model of human HSC recovery from inflammatory stress.

Results:

Unperturbed LT-HSCs exhibit heterogeneous transcriptional priming for response to inflammation

Heterogeneity among human LT-HSC has been documented in the context of cell cycle priming, with HSC ranging from deeply quiescent to those that are primed for cell cycle entry (*23*). To specifically interrogate LT-HSC variation in transcriptional programs, we performed scRNA-seq on umbilical cord blood (CB) LT-HSC, defined as Lin- CD34+ CD38- CD45RA- CD90+ CD49f+, using the BD Rhapsody platform (Fig. 1A). Consensus non-negative matrix factorization (cNMF) (*42*) was implemented to identify gene expression programs that vary across sc transcriptomes of 3280 unperturbed LT-HSC. We identified distinct gene expression programs relating to quiescence (Fig. 1B), cell cycle priming (Fig. 1C) (*5*, *22*), and two programs related to inflammatory signaling including AP-1 targets (Fig. 1D) and TNFα via NF-κB signaling (Fig. 1E).

To validate our findings, we generated a combined sc transcriptome and chromatin accessibility data set of single donor CB HSPC (n=2 females, n=2 males) with the 10x 'Chromium Single Cell Multiome ATAC + Gene Expression' platform (hereafter 10x scMultiome). Profiles of 24,007 single cells that passed both RNA and ATAC quality control (QC) were retained. To purify HSCs *in silico* from this dataset, we utilized a single cell hematopoietic reference map (hereafter BoneMarrowMap, unpublished; github.com/andygxzeng/BoneMarrowMap), and validated that transcriptional HSC in BoneMarrowMap are concordant with immunophenotypic LT-HSC through projection of the CB LT-HSC scRNA-seq profiles (SFig. 1A-B). Applied to the CB Multiome data, 7,554 HSCs were purified *in silico* wherein cNMF analysis of their transcriptomes recovered similar gene expression programs corresponding to quiescence and inflammatory signaling (SFig. 1C-E). These data and previous findings (*5*–*7*, *23*) indicate HSC heterogeneity in inflammation-naive CB, with individual HSC showing variable levels of priming for inflammatory response.

In vivo modeling of inflammatory insult and subsequent recovery of human HSC

There are limited *in vivo* studies on human HSC response to inflammation. To investigate the functional impact of inflammatory stress on human HSC heterogeneity *in vivo*, we focused on tumor necrosis factor α (TNFα). Elevation of circulating TNFα has been linked to an increased risk for mortality from sepsis, COVID-19, advanced age, and age-related diseases (*43*–*46*). TNFα signaling has also been shown to regulate human and murine

HSC proliferation and survival (*10*, *31*, *47*). We confirmed that *ex vivo* TNFα treatment specifically restrains quiescence exit of CB LT-HSC, but not of downstream HSPC populations (SFig. 2A-B) (*11*). Additionally, *ex vivo* TNFα exposure for 4 days also changed the clonogenic capacity of LT-HSC (SFig. 2C-D).

We adopted a xenotransplantation model as an experimental system to evaluate how acute inflammation affects human HSC and their molecular programs following recovery *in vivo*. We first established that intraperitoneal injection of human TNFα (hTNFα) and lipopolysaccharide (LPS), which mimics sepsis (*48*), could provoke acute inflammatory responses on a human graft (Fig. 1F). We selected two timepoints post-engraftment to test, 6 weeks (w) (Fig. 1G-H and SFig. 3B-C) and 20w (Fig. 1I-J and SFig. 3D-E), where the engrafted human HSC are mostly cycling versus quiescent, respectively, as a consequence of transplantation (*23*). Human CD45+ cells were reduced 16 hours after treatment either at 6w (Fig. 1G and SFig. 3B) or 20w (Fig. 1I) post-engraftment, as was the proportion of CD34+ cells (Fig. 1H, J, SFig. 3C, E). Neither B cell nor total myeloid output were dramatically altered (Fig. S4C-D and G-H) but a significant reduction in CD14+ monocytes was observed upon treatment with LPS in both 6w and 20w mice (Fig. S4A-B and E-F). By contrast, human engraftment within the non-injected bone marrow compartment showed variable response to acute inflammation at 6w vs 20w (SFig. 3B-E) suggesting differential acute response to inflammatory events of HSC that had successfully migrated and engrafted distal sites; this may be related to cell cycle priming and heterogeneity in HSC engraftment patterns in xenografts (*6*). These findings validate hTNFα and LPS as inflammatory stimuli in a CB xenograft model.

Next, we sought to understand whether CB xenografts can recover from inflammatory insults. We performed a single challenge with PBS, hTNFα, or LPS at 2w post-engraftment, and subsequently analyzed human engraftment patterns at 20w post-engraftment (Fig. 1K). Interestingly, overall engraftment in the PBS-injected controls compared to LPS or hTNFα treated mice were similar (Fig. 1L-M, SFig. 3G-H) demonstrating that human grafts are capable of recovering from a single acute inflammatory insult as found in the murine system (*24*). No significant differences in lineage distribution were observed (SFig. 4I-L). Furthermore, secondary limiting dilution engraftment assays (LDA) into NSG-SGM3 mice did not reveal any statistically significant differences in stem cell frequency between PBS, hTNFα, or LPS conditions from a single inflammatory challenge (SFig. 3I-K).

To assess the impact of repeated infection on human HSC function, we developed a dual-challenge model wherein xenografted NSG mice were treated with PBS, hTNFα, or LPS at 2w and 10w post-engraftment followed by a 10w recovery period (Fig. 1K). Strikingly, the human graft size at 20w post-engraftment remained significantly lower with either LPS or hTNFα dual challenge compared to PBS control mice despite the recovery period

(Median engraftment for PBS: 56.60%; hTNFα: 29.60%, p <0.001; LPS: 21.20%, p <0.001, Mann-Whitney test; Fig. 1N). Lineage distribution within the human graft was variable and inconsistent between PBS control and recovery from dual challenge with LPS or hTNFα for B, myeloid or CD34+ cells in the human grafts (Fig. 1O and SFig. 4M-P). Notably, an increase in the proportion of CD3+ T cells was observed upon recovery from LPS or hTNFα at the expense of CD19+ B cells (SFig. 4O-P), and CapTCR-seq showed that this increased proportion in T cells was not due to clonal expansion (SFig. 4Q-R). We further asked whether the microenvironment impacted human HSC response to dual inflammatory challenge by adapting our model to NSGW41 mice (SFig. 5A). Endogenous murine HSC are impaired due to Kit deficiency in NSGW41 mice thereby allowing human HSC engraftment without irradiation (*49*). Robust human CD45+ leukocytic, and human GlyA+ erythrocytic grafts were obtained 20w post-engraftment, which were significantly reduced after recovery from dual LPS or hTNFα challenge in both the injected femur and non-injected bone marrow (SFig. 5B-G). No significant changes in CD34+ cells or mature lineages were observed in either compartment (SFig. 5H-M). Thus, reconstitution by human HSC is significantly reduced *in vivo* following recovery from dual inflammatory challenge, and irradiation was not a technical issue that was influencing the functional responses we observed in our xenograft models.

We performed secondary LDA (Fig. 1P) and found that secondary engraftment ability was preserved following dual inflammatory challenge, with modest increase in LPS-treated mice (Fig. 1Q-S). This is in contrast to mouse models of chronic inflammation in which HSC failed to recover functional potency up to a year after inflammatory challenge (*24*, *33*). Altogether, our dual inflammatory challenge model reveals lasting functional impairment of xenografted human HSC in the primary transplant despite the 10 week recovery period.

Two HSC compartments with distinct transcriptional and epigenetic states identified by single cell Multiome

To understand the molecular basis of the decreased human graft size observed with dual inflammatory challenge, immunophenotypic CD45+ CD34+ CD38- CD45RA- HSPC (Prim) were isolated from NSG xenografts at 20w (Fig. 1N and SFig. 3M) and subjected to 10x scMultiome profiling (Fig. 2A). Profiles of 27,492 single cells that passed both RNA and ATAC QC were retained, and cell-type assignment was guided by projection and classification through BoneMarrowMap (SFig. 6A-C). Notably, cell composition by transcriptome did not fully align with the expected composition within a typical sorted Prim population (SFig. 6B-C). Specifically, we expected most committed progenitors to be excluded, per previous published scRNA-seq data within primitive populations (*6*). Rather, transcriptomes corresponding to immunophenotypic CD38+ progenitors including

GMP, MEP, and CLP were identified (SFig. 6C-D), suggesting immunophenotypes that identify human HSPC exhibit some degree of plasticity following xenotransplantation.

Unexpectedly, we observed two HSC populations among single cells classified as HSC, hereafter denoted HSC-I and HSC-II (Fig. 2B and SFig. 6E). We similarly observed a separate MPP and LMPP population contiguous with HSC-II, hereafter referred to as MPP-II and LMPP-II. Both HSC-I and HSC-II displayed enrichment of LT-HSC-specific transcriptional (Fig. 2C and SFig. 6F) and chromatin-based (Fig. 2D and SFig. 6G) signatures derived from prior bulk sequencing datasets of purified HSPC, and share specific stem cell-specific markers relative to their downstream MPP and LMPP populations including *MECOM*, *AVP*, and *CRHBP* (SFig. 6H-K) confirming their identity as HSC (*7*, *22*, *50*).

Notably, single cell neighborhood analysis suggested that HSC-I and HSC-II constituted distinct transcriptional and epigenetic states in the context of our inflammation-recovery model. Parallel analyses with alternative scRNA and scATAC analysis pipelines including OCAT (SFig. 7A-C) (*51*), TooManyCells (SFig. 7D-F) (*52*), and TooManyPeaks (SFig. 7G-I) (*53*) provided further support that HSC-I and HSC-II constitute distinct cellular states. Compared to HSC-I, HSC-II displayed enrichment of a signature of quiescence within human LT-HSCs (Fig. 2E) as well as for genes corresponding to TNFα via NFkB signaling (Fig. 2F). Furthermore, pathway analysis revealed diverse biological pathways significantly enriched in HSC-II spanning immune and TGFβ signaling, proteostasis and stress response, and regulation of cell cycle and cell motility, while no biological pathways were significantly enriched in HSC-I (SFig. 8). In addition to differences in expression of individual genes and accessibility of individual chromatin peaks between the populations, we sought to understand whether HSC-I and HSC-II were governed by distinct gene regulatory networks (GRNs). To this end we employed SCENIC+ to integrate paired gene expression and chromatin accessibility information from individual cells towards constructed high-confidence GRNs. By integrating expression-derived TF-to-gene relationships with chromatin-derived TF-to-peak relationships and scMultiome-derived peak-to-gene relationships, this approach yields “e-Regulons” for each TF comprised of chromatin regions they bind to and nearby gene targets that they regulate through those regions (SFig. 9A-B). Using this approach we identified key TFs underlying HSC-I and HSC-II state on the basis of both chromatin accessibility and gene expression (Fig. 2G-H). Key HSC-I TFs include *HMGA2*, *MECOM*, and *MEIS1*, as well as *GATA2*, *GATA1*, and *KLF1*. Key HSC-II TFs include *NFKB1* (Fig. 2I), *NFKB2*, *REL*, as well as *JUNB* (Fig. 2J), *JUND*, *FOS*, and *FOSB*. and Further, by considering cis-regulatory relationships between differentially enriched TFs within our data, we also constructed TF-driven GRNs specific to HSC-I and HSC-II (Fig. 2K-L).

Collectively, this data suggests that the two human HSC populations observed within our inflammatory-recovery model are transcriptionally and epigenetically distinct from each other, and their states are maintained by different underlying GRNs.

HSC-II harbors memory of prior inflammatory stress

Having established that HSC-I and HSC-II are distinct stem cell populations regardless of which treatment they encountered *in vivo,* and that core inflammatory TF activity is only seen in HSC-II, we sought to understand the molecular impact of prior inflammatory stress on each HSC subset. HSC-I and HSC-II remained transcriptionally and epigenetically distinct within the PBS control xenografts, but the extent of these differences became more pronounced following prior inflammatory treatment (Fig. 3A). More specifically, quantification with Augur (*54*) revealed stronger separation of HSC-I and HSC-II by gene expression and chromatin accessibility in the context of prior hTNFα or LPS challenge compared to PBS controls (Fig. 3B).

We next asked whether HSC-I and HSC-II differed in the transcriptional and epigenetic changes they retained after inflammatory stress. To this end, we performed differential enrichment analysis of epigenetically and transcriptionally inferred TF activity from SCENIC+ (*55*) We compared HSC recovered from hTNFα or LPS treatment against PBS control, respectively. We observed that HSC-II cells that had endured prior hTNFα challenge displayed higher activity of 30 TFs after recovery, including *NFKB1* and *JUNB*, on the basis of both target region accessibility and target gene expression when compared to HSC-II from PBS controls (Fig. 3C-E). By contrast, HSC-I cells exhibited no differences in TF activity after recovery from hTNFα treatment beyond an AUC specificity threshold of 0.6. Differences in TF activity between HSC that endured LPS challenge versus PBS-treated controls were also most pronounced in HSC-II, where activity of 28 TFs, including *HMGA1*, *SPI1*, *IRF1*, and *MYC*, were enriched (Fig. 3F-H). However, in contrast to hTNFα-challenged HSC, an upregulation of *HOXA10* activity was observed in the context of LPS recovery specifically in HSC-I (Fig. 3F-H); other TFs did not consistently differ in activity at the level of both RNA and chromatin. In summary, the vast majority of the epigenetic and transcriptional changes in HSC following recovery from inflammation occurred within the HSC-II compartment, suggesting that HSC-II preferentially retains epigenetic and transcriptional memory of prior inflammatory stress. Given these findings, we hereafter refer to HSC-II as inflammatory-Memory HSC (HSC-iM) (*56*–*58*)

HSC-iM share core molecular programs with memory T cells

Immune memory is best understood in the context of T cells (*59*). We asked whether the distinct inflammatory memory state identified in HSC from our xenografts bears any resemblance to functionally-defined immunologic memory in T cells. We re-analyzed

RNA-seq and ATAC-seq data from a study where antigen-specific CD8 Memory T cells (T-mem) were purified 4-13 years after human volunteers received yellow fever vaccines (Fig. 4A) (*60*). We compared T-mem to CD8 Effector T cells (T-eff, purified 14-28 days following vaccination) as well as Naive CD8 T cells (naive-T) purified prior to vaccination (*60*). We observed high concordance in motif enrichment (R=0.77, p<2.2e-16) when comparing open chromatin regions specific to long-term T-mem against those specific to HSC-iM (Fig. 4B). In particular, AP-1 family TF binding sites defined by a core 7-bp motif - 5'-TGAG/CTCA-3' - were highly enriched in chromatin regions specific to both HSC-iM and T-mem (Fig. 4B). Conversely, EOMES and TBX21 (T-bet) motifs were specific to T-mem, as expected (*61*), albeit exhibiting modest enrichment compared to AP-1 members (Fig. 4B)(*61*).

We next asked whether open chromatin regions specific to HSC-iM (Fig. 4C) were also enriched in T-mem compared to T-eff and naive-T. Indeed, differentially accessible peaks specific to HSC-iM were enriched in T-mem (Fig. 4D) compared to T-eff (p=0.012) and naive-T (p=0.0044). Similarly, a transcriptional signature specific to HSC-iM (Fig. 4E) was enriched in T-mem relative to T-eff (p = 0.036) and naive-T (p=0.0043) (Fig. 4F). As further validation, we derived a human T-mem transcriptional signature comprised of 257 genes upregulated in T-mem compared to both naive-T and T-eff cells (Fig. 4G), and scored this signature within our xenograft data. Strikingly, the T-mem signature was highly specific to HSC-iM compared to HSC-I within our dataset (Fig. 4H; AUC=0.963), and the ability of this signature to discriminate between HSC-iM and HSC-I was most pronounced within the hTNFα (AUC=0.987) and LPS (AUC=0.965) recovery conditions compared to PBS control (AUC=0.908). Together, these data suggest core similarities between epigenetic and transcriptional programs underlying inflammatory memory in human HSC and functionally defined human T cell immune memory.

Clinical validation of an inflammatory memory program in HSC following severe COVID-19 illness

To gain insight into the clinical relevance of our findings, we considered an important and unprecedented setting where patients experience severe COVID-19 illness, which can be associated with cytokine storms, contributing to the need for hospitalization and intensive care (*44*, *62*). We evaluated paired transcriptome and chromatin accessibility profiles of 10x scMultiome-profiled HSPC collected from donors 2-4 months following intensive care unit (ICU) hospitalization either due to severe COVID-19 (Severe COVID-19-recovered; n=4) or due to other causes (ICU-recovered control; n=6), alongside HSPCs from healthy donors (Healthy control; n=7; Fig. 4I) (*62*). After *in silico* purification of HSC through BoneMarrowMap (SFig. 10), we evaluated each condition for enrichment of our HSC-iM signature at the level of both chromatin accessibility and gene expression. By chromatin accessibility, HSC from Severe COVID-19 recovered donors were enriched for the HSC-

iM chromatin signature compared to HSC from Healthy controls (p=2.1e-54) and ICU-recovered controls (p=6.3e-72) (Fig. 4J). By gene expression, HSC from Severe COVID-19- recovered donors were enriched for the HSC-iM transcriptional signature compared to HSC from ICU-recovered controls (p=1.7e-39) and Healthy controls (p=3.3e-54) (Fig. 4K). As further validation, we identified 49 differentially expressed genes unique to Severe COVID-19-recovered HSC compared to Healthy control HSC (Fig. 4L), and derived a Post-COVID HSC transcriptional program. This Post-COVID HSC program was highly specific to HSC-iM compared to HSC-I within our xenograft data (Fig. 4M; AUC=0.904), and separation based on this program was more pronounced within the hTNFα (AUC=0.927) and LPS (AUC=0.903) recovery conditions compared to PBS control (AUC=0.888). Thus, the HSC-iM signature is relevant to a setting of infection in humans.

Inflammatory memory accumulates in human HSC with age

Repeated inflammatory insults through acute infections occur throughout the human lifespan. As “inflammaging” - chronic, low-grade inflammation - develops with physiological aging, we asked whether the HSC-iM signature accumulates in human HSC across the human lifespan (*63*). To this end, we analyzed a 10x scMultiome bone marrow CD34+ HSPC data set comprised of two older-aged (OA; 70-80yr), two middle-aged (MA; 50-60yr), and two young adult (YA; 20-30yr) donors that we generated (*64*). We sought to minimize donor-specific effects by supplementing our analysis with additional published scRNA-seq datasets of human HSPCs from OA, MA, and YA donors: Ainciburu *et al.* comparing three OA (60-80yr) against three YA (20-30yr) donors (*65*), Zhang *et al.* comparing three OA (60-80yr) against two YA (20-30yr) donors (*66*), and published data sets within BoneMarrowMap comparing 14 MA (40-60yr) against 19 YA (18-40yr) donors (*67–70*). With the exception of data already included in the BoneMarrowMap, HSC were identified from these datasets through BoneMarrowMap projection (SFig. 11).

Comparing HSCs from OA or MA donors (aged) to HSC from YA donors (young) within these four datasets, we find that the HSC-iM signature is significantly enriched in aged HSC by GSEA analysis (Fig. 5A). In contrast, an HSC-I signature exhibited variable patterns of enrichment between young and aged HSC in a dataset-dependent manner (SFig. 11). To evaluate whether this association was reciprocated, we identified aging-specific HSC signatures through differential expression (DE) analyses comparing young and aged HSC within each dataset (Suppl Methods). DE genes unique to aged HSC from each dataset were significantly enriched in HSC-iM relative to HSC-I within our xenograft data by GSEA (Fig. 5B). In contrast, signatures of young HSC, which could only be obtained from two of the four datasets due to low numbers of DE genes, exhibited variable enrichment between HSC-iM and HSC-I (SFig. 11).

Finally, we sought to further minimize donor and dataset-driven variability by defining a meta-signature of human HSC aging based on 40 upregulated genes with the highest average significance across all comparisons and datasets (Suppl Methods, Fig. 5C). This signature was highly enriched in HSC-iM compared to HSC-I at the single cell level (Fig. 5D; AUC=0.906). Thus, our analysis of these independent datasets all show that molecular changes associated with HSC aging correlate with our HSC-iM signature.

Inflammatory memory drives non-cell-autonomous gene expression changes in clonal hematopoiesis

The association between our HSC-iM signature with human HSC aging prompted us to ask whether inflammatory memory may be involved in CH, a condition which is associated with both aging (*71*, *72*) and elevated serum levels of inflammatory cytokines (*26*). To understand whether inflammatory memory in human HSC is associated with CH, we investigated TARGET-seq+ data from our CH study of nine *DNMT3A* or *TET2*-mutated CH donors and four age-matched non-CH controls (Fig. 5E) (*64*). TARGET-seq+ enables simultaneous single-cell profiling of transcriptome, genotype, and FACS immunophenotype, enabling comparisons of mutant (CH^{MUT}) and wildtype (CH^{WT}) HSCs in CH with non-CH HSCs from age-matched controls (non-CH). Among 4,951 transcriptional HSC/MPP from this TARGET-seq+ cohort, we first validated that enrichment of the HSC-iM signature was correlated with age across the thirteen donors within this cohort (R =0.69, p=0.0085, Fig. 5F).

We next compared HSC/MPP from 9 CH donors against HSC from 4 non-CH control donors after adjusting for donor ID, donor age, donor sex, and FACS gate as covariates (Fig. 5E). CH^{WT} and CH^{MUT} HSC from both *DNMT3A* and *TET2* CH donors were significantly enriched for the HSC-iM signature compared to non-CH HSC (Fig. 5G). Further, we found downregulation of an HSC-I signature in the context of both CH^{WT} and CH^{MUT} HSC from *DNMT3A* donors and CH^{WT} HSC from *TET2* CH donors compared to non-CH HSC (Fig. 5H). The observation that these enrichment patterns persist in both CH^{WT} and CH^{MUT} HSC suggests a non-cell-autonomous role for inflammatory memory in the context of CH. In order to benchmark the relative significance of these associations, we extended our GSEA analysis to incorporate 7,341 additional biological pathways and literature genesets from MSigDB, and ranked the enrichment results based on statistical significance. Strikingly, enrichment for the HSC-iM signature surpassed all other genesets by statistical significance for all four comparisons contrasting CH^{WT} or CH^{MUT} HSC from *DNMT3A* or *TET2* donors against non-CH HSC (Fig. 5I). Thus, inflammatory memory was the biological property that best captured non-cell-autonomous differences between HSC in CH donors versus HSC from non-CH controls.

We then asked whether our HSC-iM signature differed between CH^{WT} or CH^{MUT} HSC within each CH donor. Comparing CH^{MUT} against CH^{WT} HSC after adjusting for donor ID and FACS sorting as covariates in CH donors, we found that the HSC-iM signature was further enriched in CH^{MUT} compared to CH^{WT} HSC (Fig. 5J). While still significant, the strength of these associations were more modest, with the HSC-iM signature ranking as #10 and #9 out of 7,343 genesets evaluated in *DNMT3A* and *TET2*, respectively. These data indicate that an additional clone-specific role for inflammatory memory may underlie selective advantage in both *DNMT3A* and *TET2* CH in response to an inflammatory milieu. In summary, we found that HSC-iM is enriched in HSC from individuals with CH regardless of genotype, implying molecular changes stemming from inflammation underlie non-cell-autonomous changes in both CH^{WT} and CH^{MUT} HSC.

Modeling of inflammation-recovery in xenografts recapitulates HSC states in aging and clonal hematopoiesis

Given the strength of enrichment patterns for HSC-iM in the context of CH, our CH data set presented an opportunity to ask if HSC-I and HSC-iM could be identified in an unbiased manner from human adults where functionally validated immunophenotypic markers (*73*) were used to isolate HSPC. In our separate CH study (*64*), we had performed unsupervised feature selection and clustering using the Self-Assembling Manifolds (SAM) tool on primitive HSPC, which revealed three clusters of human HSC within the cohort, termed HSC1, HSC2, and HSC3 (Fig. 6A). The ratio of HSC2 to HSC1 cells varied extensively across donors, although the ratio was higher among CH donors compared to control donors (p=0.046) (Fig. 6B,C). We investigated whether the HSC subsets identified in human adult CH bone marrow were comparable to the HSC-I and HSC-iM subsets reported from our xenotransplantation models. HSC1 was highly enriched for a HSC-I signature as defined by the xenograft data (vs HSC2; AUC=0.944) while HSC2 was highly enriched for the HSC-iM signature from the xenograft data (vs HSC1; AUC=0.963) (Fig. 6D). Reciprocally, a gene expression signature representing HSC1 from the CH dataset was highly specific to the HSC-I population from the xenograft dataset (vs HSC-iM; AUC=0.964) and a signature representing HSC2 was highly specific to HSC-iM (vs HSC-I; AUC=0.992) (Fig. 6E). Thus, HSC1 and HSC2, identified from TARGET-seq+ profiles of bone marrow HSPCs from CH donors and non-CH controls, are equivalent to the HSC-I and HSC-iM subsets identified by 10x scMultiome profiling of xenografted CB HSPC. Note that HSC3 within the CH data exhibited intermediate enrichment of both HSC-I and HSC-iM signatures, potentially representing a transitional population between these key HSC states (SFig. 12). To confirm we had identified HSC-I and HSC-iM *de novo* in the CH data set, we analyzed HSC-I and HSC-iM signature enrichment of cells belonging to each of the three HSC clusters from non-CH and CH donors separated by CH^{WT} or CH^{MUT} status (Fig. 6F). Non-CH, CH^{WT}, and CH^{MUT} HSC span a transcriptional gradient of HSC-iM signature enrichment. Notably, there is an

overall shift in signature strength within CH^{MUT} HSC towards the HSC-iM state compared to other conditions, highlighting the relevance of inflammatory memory in CH (Fig. 6F).

To interrogate the cell-autonomous impact of CH mutations in the context of HSC-I and HSC-iM, we analyzed clone-specific gene expression changes of *DNMT3A* or *TET2* CH within each HSC subset (Fig. 6G). Differential expression analysis between CH^{MUT} and CH^{WT} cells within CH donors revealed that gene expression changes occurred predominantly within the HSC2 cluster for both *DNMT3A* and *TET2* donors (Fig. 6H). Further, comparison of TF regulon enrichment between CH^{MUT} and CH^{WT} cells identified dysregulated TF activity exclusively in HSC2 for both *DNMT3A* and *TET2* (Fig. 6I). These results bear similarity to our *in vivo* inflammation-recovery model wherein differences between experimental conditions occurred predominantly within the HSC-iM population (Fig 3C-H). Collectively, this data shows that clone-specific transcriptional dysregulation enacted by CH mutations occur predominantly within the HSC-iM state.

Discussion

Here we report that the human LT-HSC pool is more heterogeneous than previously anticipated by discovering a new HSC subset, termed HSC-iM, which retains transcriptional and epigenetic memory of prior inflammation. HSC-iM is highly concordant with well-established signatures associated with human T cell memory pointing to convergence between these disparate cell types. Further support for the concept of conserved memory programs among stem cells and immune cells comes from the recently reported inflammatory memory in epidermal stem cells (*56–58*). Although identified in a xenograft model, HSC-iM and their underlying programs are highly relevant in three clinical settings: HSC-iM are highly enriched in patients following severe COVID-19 illness; HSC-iM accumulate as humans age; and HSC-iM programs are highly associated with both CH^{WT} and CH^{MUT} HSC. Thus, HSC-iM represents an HSC reservoir that captures inflammatory events across a lifetime and provides a basis for how inflammation may drive age-related changes in the HSC pool and cause erosion of HSC fitness.

Inflammation activates stem cells, and over a lifetime can severely disrupt stem cell fitness (*24*, *33*). Age-related increase in inflammation is a well-recognized major risk factor for many diseases, including cancer, cardiovascular disease, chronic liver disease, autoimmune disease, and diabetes (*71*, *72*, *74–76*). Aging is also the greatest risk factor for CH, where mutations that confer a selective growth advantage result in expansion of mutated hematopoietic cells in the blood and in various tissues in the body (*71*, *72*, *76*). CH has a prevalence of approximately 1 in 5 in people over 60 years of age (*71*, *72*, *76*). Separately from age, CH results in a 12-fold increased risk for blood cancers, cardiovascular disease, and other diseases associated with human aging (*71*, *72*, *75*, *76*).

But whether inflammation directly drives deleterious molecular changes within HSC and subsequently impacts human health and longevity was not previously known. The mechanisms that underlie the selection of CH mutant clones are also not clear. By establishing an inflammation-recovery xenotransplantation model that is able to recapitulate HSC states found in aging and CH, we have begun to provide clues to these important questions. Critically, the HSC-iM subset identified from our xenograft model is equivalent to an HSC subset found in adult BM from our separate CH study (*64*). We propose that CH mutations have both cell-autonomous and non-cell-autonomous effects on HSC, wherein they affect both CH^{MUT} and CH^{WT} cells. Our finding that HSC-iM enrichment occurs in CH donors regardless of genotype suggests that individuals with CH have had greater exposure to, or are more impacted by "inflammaging". We further hypothesize that the mutation may either be promoting an inflammatory environment or it is selected for in the context of inflammatory memory. As clone-specific transcriptional dysregulation in CH^{MUT} occurs predominantly within HSC-iM, it may within this state that the mutation provides a competitive advantage. An attractive hypothesis is that there is a greater risk for transformation from a preleukemia state to disease when a somatic mutation arises in HSC-iM (*77*). Together with increasing evidence that CH mutations arise early in life (*25–28*), the discovery of HSC-iM raises the question of how an inflammatory memory background may influence the selective fitness of a CH mutant clone.

We propose that the HSC-iM subset emerges as a 'cost' of adaptation to inflammation for HSC pool maintenance (*77*, *78*). HSC are wired to prevent damage from being propagated; in some settings like low-dose radiation or proteostatic stress they are culled more efficiently (*79*, *80*). Here, we hypothesize that repeated inflammatory stress drives the affected HSC into dormancy as a protective adaptation (that is, providing beneficial effects in the short-term to protect the integrity of the stem cell pool over a lifetime) (*78*, *81*). Support for this concept comes from a distinguishing feature of HSC-iM where their transcriptional and epigenetic state is concomitantly enriched for inflammation response and a LT-HSC quiescence vs activation signature (Fig. 2E-F) (*5*). However, the cell cycle kinetics of HSC-iM are unknown. Nonetheless, the existence of two distinct HSC states adds nuance to our understanding of clonal evolution and selective advantages in HSC. We wonder whether the enrichment of HSC-iM during aging provides a reservoir of cells from which one HSC can acquire the CH mutation to gain selective advantage in an inflammatory milieu. Alternatively, a CH mutation could occur in an HSC-I cell, and the mutation then promotes transition to the HSC-iM state. To understand the loss of clonal diversity in age (*19*) or expansion of mutant clones in CH, we would need to model the impact of a CH mutation on HSC-iM. However, this will require prospective isolation of HSC-iM, something which is currently not possible as we can only infer their presence retrospectively through transcriptional and/or epigenetic profiling. Thus, while we have deeply characterized the molecular characteristics and phenotypic associations of this

novel inflammatory memory HSC subset, many additional questions remain. Future functional studies are required to complement the computational signatures we found here for which we need immunophenotypic markers for prospective isolation of HSC-iM. Furthermore, we do not know if HSC-I and HSC-iM originate from the same pool of HSC, nor do we know whether they are static or dynamic states, which may be addressed with lineage tracing (*82*). In summary, we have established an inflammation-recovery xenotransplantation model and an inflammatory memory framework to mechanistically interrogate the role of HSC in infection, aging and disease.

Acknowledgments: We thank the obstetrics unit of Trillium Health, William Osler and Credit Valley Hospitals for CB; K.B.K, Q.L. and N.M. for help with intra-femoral injections; The UHN-Sickkids Flow cytometry facility for cell sorting and The Princess Margaret Genomic Centre for 10x Multiome library prep and sequencing.

Funding: A.G.X.Z. is supported by a University of Toronto MD/PhD studentship award. S.Z.X. is supported by funds from the Princess Margaret Cancer Foundation. Work in the laboratory of J.E.D. is supported by funds from the Princess Margaret Cancer Foundation, Ontario Institute for Cancer Research through funding provided by the Government of Ontario, Canadian Institutes for Health Research (RN380110-409786), International Development Research Centre Ottawa Canada, Canadian Cancer Society (703212), a Terry Fox New Frontiers Program project grant, University of Toronto's Medicine by Design initiative with funding from the Canada First Research Excellence Fund, the Ontario Ministry of Health, and a Canada Research Chair. P.V. acknowledges funding 574 from the Medical Research Council Molecular Haematology Unit Programme Grant (MC_UU_00029/8), Blood Cancer UK Programme Continuity Grant 13008, NIHR Senior Fellowship, and the Oxford Biomedical Research Centre Haematology Theme. N.A.J. was supported by a Medical Research Council and Leukaemia UK Clinical Research Training Fellowship (MR/R002258/1).

Author contributions. Conceptualization, S.Z.X.; Methodology, S.Z.X., A.G.X.Z., M.S.N, and N.A.J.; Investigation, S.Z.X., A.G.X.Z., M.S.N, I.L., L.J, J.A., D.P., J.M., H.K., M.B., E.W.; Formal analysis, A.G.X.Z., N.A.J., S.S., A. M., and J.G.C.; Visualization, A.G.X.Z., N.A.J. and S.S.; Resources, A.G.A.N and E.F.F.; Supervision, S.Z.J., P.V., J.E.D, and S.Z.X.; Funding acquisition, P.V., J.E.D., and S.Z.X.; Writing - Original Draft, A.G.X.Z., M.S.N, J.E.D., and S.Z.X; Writing - Review & Editing, all authors.

Competing interests. J.E.D. serves on the SAB for Graphite Bio, receives royalties from Trillium Therapeutics Inc/Pfizer and receives a commercial research grant from Celgene/BMS.The remaining authors declare no competing interests.

Main Materials and Methods:

Human cord blood (CB) samples

Human CB samples were obtained with informed consent from Trillium Health, Credit Valley and William Osler Hospitals (Toronto, ON) according to procedures approved by the University Health Network (UHN) Research Ethics Board. Mononuclear cells (MNC) from pools of male and female CB (~1-8 donors) were obtained by centrifugation over a density barrier of Lymphoprep (Multicell, Canada). After red cell lysis with ammonium chloride (STEMCELL, Vancouver, BC) MNCs were enriched for hematopoietic stem and progenitor cells (HSPCs) by positive selection with the CD34 Microbead kit (Miltenyi, Germany) per manufacturer's instructions, or by lineage depletion as described (*83*). Resulting HSPC-enriched CB cells were cryopreserved in 50% PBS, 40% fetal bovine serum (FBS) and 10% DMSO and stored at -80°C short-term or -150°C long-term.

Mice

Animal experiments were done in accordance with institutional guidelines approved by the UHN Animal Care Committee. The following mouse strains (The Jackson Laboratory, Bar Harbor, ME) were used in this study: NOD.Cg-*Prkdc*^{scid} *Il2rg*^{tm1Wjl}*/SzJ* (NSG; strain 005557), NSG-Tg(CMV-IL3,CSF2,KITLG)1Eav/MloySzJ (NSG-SGM3; strain 013062), and NSG-*Kit*$^{W-41J}$/WaskJ (NSG-W41; strain 026497). All *in vivo* experiments were done with 8- to 12-week-old female or male mice. NSG and NSG-SGM were conditioned with 225cGy of gamma radiation; NSG-W41 females were not irradiated. All mice were housed at the animal facility (ARC) at Princess Margaret Cancer Centre in a room designated only for immunocompromised mice with individually ventilated racks equipped with complete sterile micro-isolator caging (IVC), on corn-cob bedding and supplied with environmental enrichment in the form of a red house/tube and a cotton nestlet. Cages were changed at least once a week under a biological safety cabinet. Health status was monitored using a combination of environmental monitoring and evaluation of soiled bedding from sentinel mice.

Fluorescence-activated cell sorting (FACS) and flow cytometry analyses

HSPC-enriched human CB cells were thawed via slow dropwise addition of X-VIVO 10 media (LONZA, Switzerland) with 50% FBS and 100µg/mL DNaseI (Roche, Switzerland). Cells were centrifuged at 400g for 10min, then resuspended in PBS+5% FBS. The populations sorted for individual experiments are indicated; populations are designated based on the full stem and progenitor hierarchy as described by Notta et al. (Notta et al., 2016). Cells were resuspended at <10×10^6 cells/mL and stained in one or two subsequent rounds for 15min at room temperature each. See Supplemental Table 1 for antibodies. Cells were washed following staining and resuspended in PBS+5%FBS and filtered through 40µm nylon mesh for sorting or analyses. To isolate xenografted

human cells, bone marrow from 3-5 mice per experimental group was thawed, pooled, mouse depleted using a MACS-based kit (Miltenyi) and stained for cell sorting. Cells were sorted on BD FACSAria Fusion, BD FACSAria III or BD Symphony S6 cell sorters, or analyzed on BD FACSCelesta or BD Symphony A1 coupled to a high-throughput system (HTS).

Cell cycle analysis

Sorted LT-HSC, ST-HSC, CMP, GMP or MEP as described (*5*). Sorted cells were cultured in low cytokine media (X-VIVO 10, supplemented with 1% BSA, L-Glutamine, Pen/Strep, and the following cytokines (Miltenyi): 100 ng/mL SCF, 100 ng/mL Flt3L, 50 ng/mL TPO and 10 ng/mL IL7) with 50 ng/mL human tumor necrosis factor (hTNF)α (Peprotech) or PBS control for 4 days, then fixed and stained for Ki67-Hoechst assays as described (*23*).

Colony assays

LT-HSC were purified by cell sorting from CB were cultured for 4 days in low cytokine media as above with or without 50 ng/mL hTNFα. Progeny of 150 cells were added into 2 mL methylcellulose (STEMCELL 4034) supplemented with 10 ng/mL each of Flt3L and IL6 (Miltenyi) and plated onto 2 x 35 mm dishes as duplicates. Colonies were scored manually at day 10-12 after plating. Colonies were washed off using PBS on day 14 and dispersed by passing through a 28g needle. Secondary cloning efficiency of 1/100th of total cells was evaluated at day 11-12 after replating.

Xenotransplantation

Following cell sorting, 8,000-10,000 CD34+CD38- cells were transplanted by intrafemoral injection into the right femur of appropriately conditioned age- and sex-matched mice in a volume of 30μL PBS. To induce acute inflammatory stress, mice were injected intraperitoneally with 5μg hTNFα or 40μg lipopolysaccharide (LPS) at the indicated time points. Control groups were injected with the vehicle control PBS. Mice were euthanized at the indicated time points by cervical dislocation and the injected femur along with other hindlimb long bones (non-injected femur and both tibias) collected into Iscove's modified Dulbecco's medium (IMDM)+5%FBS. Spleens were also collected in the same medium. Injected and non-injected bones were flushed separately in IMDM+5%FBS using a 23g needle for some experiments. Alternatively, bones from most mice euthanized at a 20w post-engraftment time point were crushed in PBS+5%FBS using a mortar and pestle and the resulting cell suspension passed through a 40-70μm nylon mesh. Spleens were macerated using a syringe plunger, then passed through a 40μm nylon mesh. Typically, 5-10% of cells were analyzed for human chimerism and lineage markers using flow cytometry; antibodies are listed in Table 1. Remaining cells were cryopreserved. For serial transplantation, xenografted cells were

sorted for human CD45 (see table 1) and transplanted into NSG-SGM mice at the indicated cell doses. A mouse was considered engrafted if human chimerism was >0.1% and LT-HSC frequency by limiting-dilution assay (LDA) was estimated using the ELDA software (http://bioinf.wehi.edu.au/software/elda/) (*84*).

T cell culture and CapTCRseq

Approximately 300,000 CD45+CD34-CD19-CD33- were isolated by FACS as described above from cryopreserved xenograft bone marrow to enrich T cells and deplete B, myeloid and progenitor cells. Cells were seeded in X-VIVO 20 media supplemented with 5% human AB serum and 30U/mL hIL-2 and stimulated with anti-CD3/CD28 Dynabeads (0.5 beads per cell) (*85*). Live cells were counted by trypan blue exclusion on a hemocytometer, and maintained in culture for 8 days before harvesting. Genomic DNA was extracted with a QIAamp DNA blood mini kit (Qiagen), quantified using a NanoDrop ONE instrument, and submitted for CapTCRseq (*86*) at the Princess Margaret Genomics Centre. Shannon's diversity index was calculated for the reads obtained for the three TCR genes as described previously (*87*).

Single Cell Multiome Sequencing

For scMultiomics analysis, cryopreserved bone marrow from xenografted mice was processed for FACS as described above and sorted for CD19-CD34+CD38-CD45RA- live cells. Human bone marrow was similarly thawed and stained for FACS and were sorted for CD19-CD34+CD38- and CD19-CD34+CD38+ populations. The two populations were pooled back together at known ratios for further processing. Sample processing including nuclei isolation and library construction was performed by the Princess Margaret Genome Centre for downstream 10x Genomics scMultiome RNA + ATAC sequencing using their low-input protocol.

Quality Control

RNA and ATAC processing was performed using Seurat and Signac, respectively, in R and applied to each sample before merging. The UMI count matrix was loaded in the R environment using Read10X. Doublets were identified using scDblFinder on the RNA. The 10x count matrix for each sample was corrected for ambient RNA contamination using SoupX, and further quality control was performed by filtering out cells above a sample-specific sample specific percent mitochondrial genes (percent.mt), nucleosome banding pattern (nucleosome_signal), and below a sample-specific ATAC transcriptional start site enrichment score (TSS.enrichment), total number of unique feature counts (nFeature_SoupX), and total number of fragments in peaks (nCount_ATAC). The single-cell RNA-seq data from Ainciburu et al. deposited in GSE180298 was pre-processed solely using the available RNA and was not corrected using SoupX.

Ainciburu et al. scRNAseq:
young1: 200 > nFeature_RNA > 4000, percent.mt > 10; young2: 200 > nFeature_RNA > 2700, percent.mt > 10; young3: 200 > nFeature_RNA > 4000, percent.mt > 5; young4: 200 > nFeature_RNA > 4000, percent.mt > 5; young5: 200 > nFeature_RNA > 5000, percent.mt > 10; elderly1: 200 > nFeature_RNA > 4000, percent.mt > 10; elderly2: 200 > nFeature_RNA > 4000, percent.mt > 10; elderlyt3: 200 > nFeature_RNA > 5000, percent.mt > 10

CordBlood scMultiome:
CBA: nFeature_SoupX < 300, percent.mt > 8, nCount_ATAC < 1000, nucleosome_signal > 2, TSS.enrichment < 1; CBB: nFeature_SoupX < 300, percent.mt > 8, nCount_ATAC < 1000, nucleosome_signal > 2, TSS.enrichment < 1

In-house Aging scMultiome:
BM24M: nFeature_SoupX < 300, percent.mt > 10, nCount_ATAC < 1000, nucleosome_signal > 2, TSS.enrichment < 1; BM26F: nFeature_SoupX < 200, percent.mt > 15, nCount_ATAC < 1000, nucleosome_signal > 2, TSS.enrichment < 1; BM57M_58F: nFeature_SoupX < 100, percent.mt > 18, nCount_ATAC < 1000, nucleosome_signal > 2, TSS.enrichment < 1; BM70F: nFeature_SoupX < 200, percent.mt > 12, nCount_ATAC < 1000, nucleosome_signal > 2, TSS.enrichment < 1; BM77F: nFeature_SoupX < 200, percent.mt > 14, nCount_ATAC < 1000, nucleosome_signal > 2, TSS.enrichment < 1

Xenograft scMultiome:
PBS: nFeature_SoupX < 1000, percent.mt > 18, nCount_ATAC < 1000, nucleosome_signal > 2, TSS.enrichment < 1; TNF: nFeature_SoupX < 1000, percent.mt > 18, nCount_ATAC < 1000, nucleosome_signal > 2, TSS.enrichment < 1; LPS: nFeature_SoupX < 1000, percent.mt > 18, nCount_ATAC < 1000, nucleosome_signal > 2, TSS.enrichment < 1

Furthermore, pooled samples with multiple donors (CordBlood Pool A and B, In-house Middle Age donors, Xenograft) were separated using SoupOrCell by running the algorithm across multiple components representing the number of distinct genotypes by scRNAseq. The optimal component was selected using an elbow plot of the total log probability. SoupOrCell also allowed us to filter out further assigned doublets with mixed genotypes and sex gene expression. The total number of cells post-quality control was used for downstream analysis.

Consensus non-negative matrix factorization

Consensus non-negative matrix factorization was run with 100 iterations on the single cells from components 2-15 to pull out transcriptional gene programs of variation in an unsupervised manner. Raw counts were fed into the –counts flag, and SCTransform V2 corrected counts specifically from the data slot of the SCT assay were fed into the –tpm flag of the cNMF command line function with 10 workers. Following running cNMF across various components, the optimal number of components was selected by assessing the silhouette score (stability) and Frobenius reconstruction error (error). Gene signatures were defined using pathway analysis with Hallmarks, GO biological pathways, C8 cell-type signatures, and in-house genesets.

Bone Marrow Reference Map Cell Type Mapping

Cells were annotated by projecting the single cell RNA sequencing datasets onto an in-house bone marrow reference map with balanced representation of HSPCs and terminally differentiated populations (https://github.com/andygxzeng/BoneMarrowMap). The HSC population was validated using the projection of scRNA-seq data of sorted LT-HSCs (Lin-CD34+CD38-CD45RA-CD90+CD49f+). First, a query object was created and the cells were mapped onto the reference map using the function map_Query while also defining the batch effect variable in the –vars slot. The mapping error was calculated and cells with high mapping error scores suggestive of low quality cells were filtered out. Next, a KNN classifier was employed, utilizing the predict_CellTypes function, to assign cell identities based on the reference map.

SCENIC+

First, the quality-controlled 27,492 single cells from the Xenograft scMultiome were downsampled to the metacell level using the divide and conquer algorithm from the Metacell2 package. The highly variable genes used to construct the uniform manifold and projection were used as input into the algorithm guiding feature gene selection, thus optimizing clustering for metacell partitioning. The approach generated 1,476 metacells with a target metacell size of 75,000 UMI. Next, pyCistopic was used to identify cell states and cis-regulatory topics from the ATAC single cells in an unsupervised manner. The ideal number of topics were evaluated using various metrics, including log-likelihood, average model coherence following Minmo et al.'s (2011) method, density-based metrics from Arun et al.'s (2010) approach, and a divergence-based metric as proposed by Cao Juan et al. (2009). Consequently, pyCistopic optimized at 18 topics. Motif enrichment analysis was subsequently carried out by leveraging pyCistarget, which utilizes precomputed databases comprising motif scores and rankings for genomic regions, and a motif-to-transcription factor annotation database sourced from the Aerts lab resources. This analysis was conducted on the topics from pyCistopic and differentially accessible regions between each defined cell type.

Following pyCistopic and pyCistarget, a SCENIC+ object was created for downstream steps to create enhancer-driven gene regulatory networks using the ATAC and RNA. First, regions and genes not present in more than 0.5% of cells were filtered out. Next, cistromes were generated using the function merge_cistromes, which overlaps targets assigned to a TF from the motif enrichment dictionaries with the regions in the SCENIC+ object. Then, enhancer-to-gene relationships were inferred by first defining the search space around each gene of 150kb upstream/downstream, specifically on the metacells, to limit memory usage while connecting to biomart host 98. After, enhancer-to-gene models were generated using gradient boosting machines with the function calculate_regions_to_genes_relationships from SCENIC+. Next, TF-to-gene relationships were inferred using pySCENIC on the RNA metacells as per the guidelines from Van de Sande et al. with a candidate list of TFs from Lambert et al. and loaded into the SCENIC+ object from a saved adjacencies matrix using the function load_TF2G_adj_from_file. Finally, enhancer-driven gene regulatory networks were generated using a GSEA recovery approach from SCENIC+ using the function build_grn. The SCENIC+ output was simplified and filtered using the function apply_std_filtering_to_eRegulons, allowing an analysis with high confidence eRegulons.

Antigen	fluorophore	company	Cat no	Species	Isotype	clone
CD10	BV421	BD	562902	Mouse	IgG1κ	HI10a
CD14	BV605	BD	564054	Mouse	IgG2aκ	M5E2
CD14	BV605	BD	564054	Mouse	IgG2aκ	M5E2
CD14	PE-Cy5	beckman coulter	IM2640U	Mouse	IgG2a	RMO52
CD19	BV711	BD	563036	Mouse	IgG1κ	SJ25C1
CD19	PE	BD	349209	Mouse	IgG1κ	4G7
CD19	PC5	beckman coulter	IM2643U	Mouse	IgG1	J3-119
CD235a	PE	beckman coulter	IM2211U	Mouse	IgG1	11E4B-7-6
CD235a	PC5	BD	559944	Mouse	IgG2bκ	GA-R2
CD3	FITC	BD	349201	Mouse	IgG1κ	SK7
CD33	BV785	Biolegend	303428	Mouse	IgG1κ	WM53
CD33	BV421	Biolegend	303416	Mouse	IgG1κ	WM53
CD34	APC-Cy7	BD	624072 (Custom	Mouse	IgG1κ	581
CD38	PE-Cy7	BD	335790	Mouse	IgG1κ	HB7
CD45	Alexa Fluor 700	BD	560566	Mouse	IgG1κ	HI30
CD45	V500	BD	560777	Mouse	IgG1κ	HI30
CD45	APC	BD	340943	Mouse	IgG1κ	2D1
CD45RA	FITC	BD	555488	Mouse	IgG2bκ	HI100
CD49f	PE-Cy5	BD	551129	Rat	IgG2aκ	GoH3
CD56	BV605	BD	562780	Mouse	IgG2bκ	NCAM16.2
CD66b	Alexa Fluor 647	BD	561645	Mouse	IgMκ	G10F5
CD7	Alexa Fluor 700	BD	561603	Mouse	IgG1κ	M-T701
CD71	FITC	BD	347513	Mouse	IgG2a	L01.1
CD83	PE	Biolegend	305307	Mouse	IgG1κ	HB15e
CD83	APC	Biolegend	305312	Mouse	IgG1κ	HB15e
CD90	APC	BD	559869	Mouse	IgG1κ	5.00E+10
CD90	PE	BD	555596	Mouse	IgG1κ	5.00E+10

References

1. T. M. Fliedner, D. Graessle, C. Paulsen, K. Reimers, Structure and function of bone marrow hemopoiesis: mechanisms of response to ionizing radiation exposure. *Cancer Biother. Radiopharm.* **17**, 405–426 (2002).

2. E. Laurenti, B. Göttgens, From haematopoietic stem cells to complex differentiation landscapes. *Nature*. **553**, 418–426 (2018).

3. R. Sender, R. Milo, The distribution of cellular turnover in the human body. *Nat. Med.* **27**, 45–48 (2021).

4. S. Z. Xie, L. Garcia-Prat, V. Voisin, R. Ferrari, O. I. Gan, E. Wagenblast, K. B. Kaufmann, A. G. X. Zeng, S.-I. Takayanagi, I. Patel, E. K. Lee, J. Jargstorf, G. Holmes, G. Romm, K. Pan, M. Shoong, A. Vedi, C. Luberto, M. D. Minden, G. D. Bader, E. Laurenti, J. E. Dick, Sphingolipid Modulation Activates Proteostasis Programs to Govern Human Hematopoietic Stem Cell Self-Renewal. *Cell Stem Cell* (2019), doi:10.1016/j.stem.2019.09.008.

5. L. García-Prat, K. B. Kaufmann, F. Schneiter, V. Voisin, A. Murison, J. Chen, M. Chan-Seng-Yue, O. I. Gan, J. L. McLeod, S. A. Smith, M. C. Shoong, D. Parris, K. Pan, A. G. X. Zeng, G. Krivdova, K. Gupta, S.-I. Takayanagi, E. Wagenblast, W. Wang, M. Lupien, T. Schroeder, S. Z. Xie, J. E. Dick, TFEB-mediated endolysosomal activity controls human hematopoietic stem cell fate. *Cell Stem Cell* (2021), doi:10.1016/j.stem.2021.07.003.

6. K. B. Kaufmann, A. G. X. Zeng, E. Coyaud, L. Garcia-Prat, E. Papalexi, A. Murison, E. M. N. Laurent, M. Chan-Seng-Yue, O. I. Gan, K. Pan, J. McLeod, H. Boutzen, S. Zandi, S.-I. Takayanagi, R. Satija, B. Raught, S. Z. Xie, J. E. Dick, A latent subset of human hematopoietic stem cells resists regenerative stress to preserve stemness. *Nat. Immunol.* **22**, 723–734 (2021).

7. N. Takayama, A. Murison, S.-I. Takayanagi, C. Arlidge, S. Zhou, L. Garcia-Prat, M. Chan-Seng-Yue, S. Zandi, O. I. Gan, H. Boutzen, K. B. Kaufmann, A. Trotman-Grant, E. Schoof, K. Kron, N. Díaz, J. J. Y. Lee, T. Medina, D. D. De Carvalho, M. D. Taylor, J. M. Vaquerizas, S. Z. Xie, J. E. Dick, M. Lupien, The Transition from Quiescent to Activated States in Human Hematopoietic Stem Cells Is Governed by Dynamic 3D Genome Reorganization. *Cell Stem Cell*. **28**, 488–501.e10 (2021).

8. Y. W. Zhang, J. Mess, N. Aizarani, P. Mishra, C. Johnson, M. C. Romero-Mulero, J. Rettkowski, K. Schönberger, N. Obier, K. Jäcklein, N. M. Woessner, M.-E. Lalioti, T. Velasco-Hernandez, K. Sikora, R. Wäsch, B. Lehnertz, G. Sauvageau, T. Manke, P. Menendez, S. G. Walter, S. Minguet, E. Laurenti, S. Günther, D. Grün, N. Cabezas-Wallscheid, Hyaluronic acid–GPRC5C signalling promotes dormancy in haematopoietic stem cells. *Nat. Cell Biol.* **24**, 1038–1048 (2022).

9. C. A. Hammond, S. W. Wu, F. Wang, M. E. MacAldaz, C. J. Eaves, Aging alters the cell cycle control and mitogenic signaling responses of human hematopoietic stem cells. *Blood*. **141**, 1990–2002 (2023).

10. I. Dybedal, D. Bryder, A. Fossum, L. S. Rusten, S. E. Jacobsen, Tumor necrosis factor (TNF)-mediated activation of the p55 TNF receptor negatively regulates maintenance of cycling reconstituting human hematopoietic stem cells. *Blood*. **98**, 1782–1791 (2001).

11. W. Wang, H. Fujii, H. J. Kim, K. Hermans, T. Usenko, S. Xie, Z.-J. Luo, J. Ma, C. L. Celso, J. E. Dick, T. Schroeder, J. Krueger, D. Wall, R. M. Egeler, P. W. Zandstra, Enhanced human hematopoietic stem and progenitor cell engraftment by blocking donor T cell-mediated TNFα signaling. *Sci. Transl. Med.* **9** (2017), doi:10.1126/scitranslmed.aag3214.

12. H. Lee-Six, N. F. Øbro, M. S. Shepherd, S. Grossmann, K. Dawson, M. Belmonte, R. J. Osborne, B. J. P. Huntly, I. Martincorena, E. Anderson, L. O'Neill, M. R. Stratton, E. Laurenti, A. R. Green, D. G. Kent, P. J. Campbell, Population dynamics of normal human blood inferred from somatic mutations. *Nature*. **561**, 473–478 (2018).

13. S. C. Castle, Clinical relevance of age-related immune dysfunction. *Clin. Infect. Dis.* **31**, 578–585 (2000).

14. J. M. Guralnik, R. S. Eisenstaedt, L. Ferrucci, H. G. Klein, R. C. Woodman, Prevalence of anemia in persons 65 years and older in the United States: evidence for a high rate of unexplained anemia. *Blood*. **104**, 2263–2268 (2004).

15. C. Kollman, S. R. Spellman, M.-J. Zhang, A. Hassebroek, C. Anasetti, J. H. Antin, R. E. Champlin, D. L. Confer, J. F. DiPersio, M. Fernandez-Viña, R. J. Hartzman, M. M. Horowitz, C. K. Hurley, C. Karanes, M. Maiers, C. R. Mueller, M.-A. Perales, M. Setterholm, A. E. Woolfrey, N. Yu, M. Eapen, The effect of donor characteristics on survival after unrelated donor transplantation for hematologic malignancy. *Blood*. **127**, 260–267 (2016).

16. J. M. Bastida, M. Cabrero, O. Lopez-Godino, M. Lopez-Parra, F. Sanchez-Guijo, L. Lopez-Corral, L. Vazquez, D. Caballero, C. Del Cañizo, Influence of donor age in allogeneic stem cell transplant outcome in acute myeloid leukemia and myelodisplastic syndrome. *Leuk. Res.* **39**, 828–834 (2015).

17. B. E. Shaw, B. R. Logan, S. R. Spellman, S. G. E. Marsh, J. Robinson, J. Pidala, C. Hurley, J. Barker, M. Maiers, J. Dehn, H. Wang, M. Haagenson, D. Porter, E. W. Petersdorf, A. Woolfrey, M. M. Horowitz, M. Verneris, K. C. Hsu, K. Fleischhauer, S. J. Lee, Development of an Unrelated Donor Selection Score Predictive of Survival after HCT: Donor Age Matters Most. *Biol. Blood Marrow Transplant.* **24**, 1049–1056 (2018).

18. A. E. DeZern, C. Franklin, H.-L. Tsai, P. H. Imus, K. R. Cooke, R. Varadhan, R. J. Jones, Relationship of donor age and relationship to outcomes of haploidentical transplantation with posttransplant cyclophosphamide. *Blood Adv*. **5**, 1360–1368 (2021).

19. E. Mitchell, M. Spencer Chapman, N. Williams, K. J. Dawson, N. Mende, E. F. Calderbank, H. Jung, T. Mitchell, T. H. H. Coorens, D. H. Spencer, H. Machado, H. Lee-Six, M. Davies, D. Hayler, M. A. Fabre, K. Mahbubani, F. Abascal, A. Cagan, G. S. Vassiliou, J. Baxter, I. Martincorena, M. R. Stratton, D. G. Kent, K. Chatterjee, K. S. Parsy, A. R. Green, J. Nangalia, E. Laurenti, P. J. Campbell, Clonal dynamics of haematopoiesis across the human lifespan. *Nature*. **606**, 343–350 (2022).

20. S. Jaiswal, B. L. Ebert, Clonal hematopoiesis in human aging and disease. *Science*. **366** (2019), doi:10.1126/science.aan4673.

21. J. C. Balandrán, A. Lasry, I. Aifantis, The Role of Inflammation in the Initiation and Progression of Myeloid Neoplasms. *Blood Cancer Discov*. **4**, 254–266 (2023).

22. S. Z. Xie, K. B. Kaufmann, W. Wang, M. Chan-Seng-Yue, O. I. Gan, E. Laurenti, L. Garcia-

Prat, S.-I. Takayanagi, S. W. K. Ng, C. Xu, A. G. X. Zeng, L. Jin, J. McLeod, E. Wagenblast, A. Mitchell, J. A. Kennedy, Q. Liu, H. Boutzen, M. Kleinau, J. Jargstorf, G. Holmes, Y. Zhang, V. Voisin, G. D. Bader, J. C. Y. Wang, Y. A. Hannun, C. Luberto, T. Schroeder, M. D. Minden, J. E. Dick, Sphingosine-1-phosphate receptor 3 potentiates inflammatory programs in normal and leukemia stem cells to promote differentiation. *Blood Cancer Discov*. **2**, 32–53 (2021).

23. E. Laurenti, C. Frelin, S. Xie, R. Ferrari, C. F. Dunant, S. Zandi, A. Neumann, I. Plumb, S. Doulatov, J. Chen, C. April, J.-B. Fan, N. Iscove, J. E. Dick, CDK6 levels regulate quiescence exit in human hematopoietic stem cells. *Cell Stem Cell*. **16**, 302–313 (2015).

24. F. Caiado, E. M. Pietras, M. G. Manz, Inflammation as a regulator of hematopoietic stem cell function in disease, aging, and clonal selection. *J. Exp. Med.* **218** (2021), doi:10.1084/jem.20201541.

25. J. S. Weinstock, J. Gopakumar, B. B. Burugula, M. M. Uddin, N. Jahn, J. A. Belk, H. Bouzid, B. Daniel, Z. Miao, N. Ly, T. M. Mack, S. E. Luna, K. P. Prothro, S. R. Mitchell, C. A. Laurie, J. G. Broome, K. D. Taylor, X. Guo, M. F. Sinner, A. S. von Falkenhausen, S. Kääb, A. R. Shuldiner, J. R. O'Connell, J. P. Lewis, E. Boerwinkle, K. C. Barnes, N. Chami, E. E. Kenny, R. J. F. Loos, M. Fornage, L. Hou, D. M. Lloyd-Jones, S. Redline, B. E. Cade, B. M. Psaty, J. C. Bis, J. A. Brody, E. K. Silverman, J. H. Yun, D. Qiao, N. D. Palmer, B. I. Freedman, D. W. Bowden, M. H. Cho, D. L. DeMeo, R. S. Vasan, L. R. Yanek, L. C. Becker, S. L. R. Kardia, P. A. Peyser, J. He, M. Rienstra, P. Van der Harst, R. Kaplan, S. R. Heckbert, N. L. Smith, K. L. Wiggins, D. K. Arnett, M. R. Irvin, H. Tiwari, M. J. Cutler, S. Knight, J. B. Muhlestein, A. Correa, L. M. Raffield, Y. Gao, M. de Andrade, J. I. Rotter, S. S. Rich, R. P. Tracy, B. A. Konkle, J. M. Johnsen, M. M. Wheeler, J. G. Smith, O. Melander, P. M. Nilsson, B. S. Custer, R. Duggirala, J. E. Curran, J. Blangero, S. McGarvey, L. K. Williams, S. Xiao, M. Yang, C. C. Gu, Y.-D. I. Chen, W.-J. Lee, G. M. Marcus, J. P. Kane, C. R. Pullinger, M. B. Shoemaker, D. Darbar, D. M. Roden, C. Albert, C. Kooperberg, Y. Zhou, J. E. Manson, P. Desai, A. D. Johnson, R. A. Mathias, NHLBI Trans-Omics for Precision Medicine (TOPMed) Consortium, T. W. Blackwell, G. R. Abecasis, A. V. Smith, H. M. Kang, A. T. Satpathy, P. Natarajan, J. O. Kitzman, E. A. Whitsel, A. P. Reiner, A. G. Bick, S. Jaiswal, Aberrant activation of TCL1A promotes stem cell expansion in clonal haematopoiesis. *Nature*. **616**, 755–763 (2023).

26. A. G. Bick, J. S. Weinstock, S. K. Nandakumar, C. P. Fulco, E. L. Bao, S. M. Zekavat, M. D. Szeto, X. Liao, M. J. Leventhal, J. Nasser, K. Chang, C. Laurie, B. B. Burugula, C. J. Gibson, A. Niroula, A. E. Lin, M. A. Taub, F. Aguet, K. Ardlie, B. D. Mitchell, K. C. Barnes, A. Moscati, M. Fornage, S. Redline, B. M. Psaty, E. K. Silverman, S. T. Weiss, N. D. Palmer, R. S. Vasan, E. G. Burchard, S. L. R. Kardia, J. He, R. C. Kaplan, N. L. Smith, D. K. Arnett, D. A. Schwartz, A. Correa, M. de Andrade, X. Guo, B. A. Konkle, B. Custer, J. M. Peralta, H. Gui, D. A. Meyers, S. T. McGarvey, I. Y.-D. Chen, M. B. Shoemaker, P. A. Peyser, J. G. Broome, S. M. Gogarten, F. F. Wang, Q. Wong, M. E. Montasser, M. Daya, E. E. Kenny, K. E. North, L. J. Launer, B. E. Cade, J. C. Bis, M. H. Cho, J. Lasky-Su, D. W. Bowden, L. A. Cupples, A. C. Y. Mak, L. C. Becker, J. A. Smith, T. N. Kelly, S. Aslibekyan, S. R. Heckbert, H. K. Tiwari, I. V. Yang, J. A. Heit, S. A. Lubitz, J. M. Johnsen, J. E. Curran, S. E. Wenzel, D. E. Weeks, D. C. Rao, D. Darbar, J.-Y. Moon, R. P. Tracy, E. J. Buth, N. Rafaels, R. J. F. Loos, P. Durda, Y. Liu, L. Hou, J. Lee, P. Kachroo, B. I. Freedman, D. Levy, L. F. Bielak, J. E. Hixson, J. S. Floyd, E. A. Whitsel, P. T. Ellinor, M. R. Irvin, T. E. Fingerlin, L. M. Raffield, S. M. Armasu, M. M. Wheeler, E. C. Sabino, J. Blangero, L. K. Williams, B. D. Levy, W. H.-H. Sheu, D. M. Roden, E. Boerwinkle, J. E. Manson, R. A.

Mathias, P. Desai, K. D. Taylor, A. D. Johnson, P. L. Auer, C. Kooperberg, C. C. Laurie, T. W. Blackwell, A. V. Smith, H. Zhao, E. Lange, L. Lange, S. S. Rich, J. I. Rotter, J. G. Wilson, P. Scheet, J. O. Kitzman, E. S. Lander, J. M. Engreitz, B. L. Ebert, A. P. Reiner, S. Jaiswal, G. Abecasis, V. G. Sankaran, S. Kathiresan, P. Natarajan, Inherited causes of clonal haematopoiesis in 97,691 whole genomes. *Nature*. **586**, 763–768 (2020).

27. N. Williams, J. Lee, E. Mitchell, L. Moore, E. J. Baxter, J. Hewinson, K. J. Dawson, A. Menzies, A. L. Godfrey, A. R. Green, P. J. Campbell, J. Nangalia, Life histories of myeloproliferative neoplasms inferred from phylogenies. *Nature*. **602**, 162–168 (2022).

28. D. Van Egeren, J. Escabi, M. Nguyen, S. Liu, C. R. Reilly, S. Patel, B. Kamaz, M. Kalyva, D. J. DeAngelo, I. Galinsky, M. Wadleigh, E. S. Winer, M. R. Luskin, R. M. Stone, J. S. Garcia, G. S. Hobbs, F. D. Camargo, F. Michor, A. Mullally, I. Cortes-Ciriano, S. Hormoz, Reconstructing the Lineage Histories and Differentiation Trajectories of Individual Cancer Cells in Myeloproliferative Neoplasms. *Cell Stem Cell*. **28**, 514–523.e9 (2021).

29. S. Haas, J. Hansson, D. Klimmeck, D. Loeffler, L. Velten, H. Uckelmann, S. Wurzer, Á. M. Prendergast, A. Schnell, K. Hexel, R. Santarella-Mellwig, S. Blaszkiewicz, A. Kuck, H. Geiger, M. D. Milsom, L. M. Steinmetz, T. Schroeder, A. Trumpp, J. Krijgsveld, M. A. G. Essers, Inflammation-Induced Emergency Megakaryopoiesis Driven by Hematopoietic Stem Cell-like Megakaryocyte Progenitors. *Cell Stem Cell*. **17**, 422–434 (2015).

30. E. M. Pietras, C. Mirantes-Barbeito, S. Fong, D. Loeffler, L. V. Kovtonyuk, S. Zhang, R. Lakshminarasimhan, C. P. Chin, J.-M. Techner, B. Will, C. Nerlov, U. Steidl, M. G. Manz, T. Schroeder, E. Passegué, Chronic interleukin-1 exposure drives haematopoietic stem cells towards precocious myeloid differentiation at the expense of self-renewal. *Nat. Cell Biol.* **18**, 607–618 (2016).

31. M. Yamashita, E. Passegué, TNF-α Coordinates Hematopoietic Stem Cell Survival and Myeloid Regeneration. *Cell Stem Cell*. **25**, 357–372.e7 (2019).

32. B. de Laval, J. Maurizio, P. K. Kandalla, G. Brisou, L. Simonnet, C. Huber, G. Gimenez, O. Matcovitch-Natan, S. Reinhardt, E. David, A. Mildner, A. Leutz, B. Nadel, C. Bordi, I. Amit, S. Sarrazin, M. H. Sieweke, C/EBPβ-Dependent Epigenetic Memory Induces Trained Immunity in Hematopoietic Stem Cells. *Cell Stem Cell*. **26**, 793 (2020).

33. R. Bogeska, A.-M. Mikecin, P. Kaschutnig, M. Fawaz, M. Büchler-Schäff, D. Le, M. Ganuza, A. Vollmer, S. V. Paffenholz, N. Asada, E. Rodriguez-Correa, F. Frauhammer, F. Buettner, M. Ball, J. Knoch, S. Stäble, D. Walter, A. Petri, M. J. Carreño-Gonzalez, V. Wagner, B. Brors, S. Haas, D. B. Lipka, M. A. G. Essers, V. Weru, T. Holland-Letz, J.-P. Mallm, K. Rippe, S. Krämer, M. Schlesner, S. McKinney Freeman, M. C. Florian, K. Y. King, P. S. Frenette, M. A. Rieger, M. D. Milsom, Inflammatory exposure drives long-lived impairment of hematopoietic stem cell self-renewal activity and accelerated aging. *Cell Stem Cell*. **29**, 1273–1284.e8 (2022).

34. Z. Li, X. Cai, C.-L. Cai, J. Wang, W. Zhang, B. E. Petersen, F.-C. Yang, M. Xu, Deletion of Tet2 in mice leads to dysregulated hematopoietic stem cells and subsequent development of myeloid malignancies. *Blood*. **118**, 4509–4518 (2011).

35. E. L. Ostrander, A. C. Kramer, C. Mallaney, H. Celik, W. K. Koh, J. Fairchild, E. Haussler, C. R. C. Zhang, G. A. Challen, Divergent Effects of Dnmt3a and Tet2 Mutations on Hematopoietic Progenitor Cell Fitness. *Stem Cell Reports*. **14**, 551–560 (2020).

36. Z. Cai, J. J. Kotzin, B. Ramdas, S. Chen, S. Nelanuthala, L. R. Palam, R. Pandey, R. S. Mali, Y. Liu, M. R. Kelley, G. Sandusky, M. Mohseni, A. Williams, J. Henao-Mejia, R. Kapur, Inhibition of Inflammatory Signaling in Tet2 Mutant Preleukemic Cells Mitigates Stress-Induced Abnormalities and Clonal Hematopoiesis. *Cell Stem Cell*. **23**, 833–849.e5 (2018).

37. F. Caiado, L. V. Kovtonyuk, N. G. Gonullu, J. Fullin, S. Boettcher, M. G. Manz, Aging drives Tet2+/- clonal hematopoiesis via IL-1 signaling. *Blood*. **141**, 886–903 (2023).

38. M. Meisel, R. Hinterleitner, A. Pacis, L. Chen, Z. M. Earley, T. Mayassi, J. F. Pierre, J. D. Ernest, H. J. Galipeau, N. Thuille, R. Bouziat, M. Buscarlet, D. L. Ringus, Y. Wang, Y. Li, V. Dinh, S. M. Kim, B. D. McDonald, M. A. Zurenski, M. W. Musch, G. C. Furtado, S. A. Lira, G. Baier, E. B. Chang, A. M. Eren, C. R. Weber, L. Busque, L. A. Godley, E. F. Verdú, L. B. Barreiro, B. Jabri, Microbial signals drive pre-leukaemic myeloproliferation in a Tet2-deficient host. *Nature*. **557**, 580–584 (2018).

39. L. I. Shlush, S. Zandi, A. Mitchell, W. C. Chen, J. M. Brandwein, V. Gupta, J. A. Kennedy, A. D. Schimmer, A. C. Schuh, K. W. Yee, J. L. McLeod, M. Doedens, J. J. F. Medeiros, R. Marke, H. J. Kim, K. Lee, J. D. McPherson, T. J. Hudson, HALT Pan-Leukemia Gene Panel Consortium, A. M. K. Brown, F. Yousif, Q. M. Trinh, L. D. Stein, M. D. Minden, J. C. Y. Wang, J. E. Dick, Identification of pre-leukaemic haematopoietic stem cells in acute leukaemia. *Nature*. **506**, 328–333 (2014).

40. E. Wagenblast, J. Araújo, O. I. Gan, S. K. Cutting, A. Murison, G. Krivdova, M. Azkanaz, J. L. McLeod, S. A. Smith, B. A. Gratton, S. A. Marhon, M. Gabra, J. J. F. Medeiros, S. Manteghi, J. Chen, M. Chan-Seng-Yue, L. Garcia-Prat, L. Salmena, D. D. De Carvalho, S. Abelson, M. Abdelhaleem, K. Chong, M. Roifman, P. Shannon, J. C. Y. Wang, J. K. Hitzler, D. Chitayat, J. E. Dick, E. R. Lechman, Mapping the cellular origin and early evolution of leukemia in Down syndrome. *Science*. **373** (2021), doi:10.1126/science.abf6202.

41. S. Abelson, G. Collord, S. W. K. Ng, O. Weissbrod, N. Mendelson Cohen, E. Niemeyer, N. Barda, P. C. Zuzarte, L. Heisler, Y. Sundaravadanam, R. Luben, S. Hayat, T. T. Wang, Z. Zhao, I. Cirlan, T. J. Pugh, D. Soave, K. Ng, C. Latimer, C. Hardy, K. Raine, D. Jones, D. Hoult, A. Britten, J. D. McPherson, M. Johansson, F. Mbabaali, J. Eagles, J. K. Miller, D. Pasternack, L. Timms, P. Krzyzanowski, P. Awadalla, R. Costa, E. Segal, S. V. Bratman, P. Beer, S. Behjati, I. Martincorena, J. C. Y. Wang, K. M. Bowles, J. R. Quirós, A. Karakatsani, C. La Vecchia, A. Trichopoulou, E. Salamanca-Fernández, J. M. Huerta, A. Barricarte, R. C. Travis, R. Tumino, G. Masala, H. Boeing, S. Panico, R. Kaaks, A. Krämer, S. Sieri, E. Riboli, P. Vineis, M. Foll, J. McKay, S. Polidoro, N. Sala, K.-T. Khaw, R. Vermeulen, P. J. Campbell, E. Papaemmanuil, M. D. Minden, A. Tanay, R. D. Balicer, N. J. Wareham, M. Gerstung, J. E. Dick, P. Brennan, G. S. Vassiliou, L. I. Shlush, Prediction of acute myeloid leukaemia risk in healthy individuals. *Nature*. **559**, 400–404 (2018).

42. D. Kotliar, A. Veres, M. A. Nagy, S. Tabrizi, E. Hodis, D. A. Melton, P. C. Sabeti, Identifying gene expression programs of cell-type identity and cellular activity with single-cell RNA-Seq. *Elife*. **8** (2019), doi:10.7554/eLife.43803.

43. P. Damas, A. Reuter, P. Gysen, J. Demonty, M. Lamy, P. Franchimont, Tumor necrosis factor and interleukin-1 serum levels during severe sepsis in humans. *Crit. Care Med.* **17**, 975–978 (1989).

44. R. Karki, B. R. Sharma, S. Tuladhar, E. P. Williams, L. Zalduondo, P. Samir, M. Zheng, B. Sundaram, B. Banoth, R. K. S. Malireddi, P. Schreiner, G. Neale, P. Vogel, R. Webby, C. B.

Jonsson, T.-D. Kanneganti, Synergism of TNF-α and IFN-γ Triggers Inflammatory Cell Death, Tissue Damage, and Mortality in SARS-CoV-2 Infection and Cytokine Shock Syndromes. *Cell*. **184**, 149–168.e17 (2021).

45. H. Bruunsgaard, K. Andersen-Ranberg, J. v. B. Hjelmborg, B. K. Pedersen, B. Jeune, Elevated levels of tumor necrosis factor alpha and mortality in centenarians. *Am. J. Med.* **115**, 278–283 (2003).

46. L. Ferrucci, E. Fabbri, Inflammageing: chronic inflammation in ageing, cardiovascular disease, and frailty. *Nat. Rev. Cardiol.* **15**, 505–522 (2018).

47. C. J. H. Pronk, O. P. Veiby, D. Bryder, S. E. W. Jacobsen, Tumor necrosis factor restricts hematopoietic stem cell activity in mice: involvement of two distinct receptors. *J. Exp. Med.* **208**, 1563–1570 (2011).

48. T. Skirecki, J. Kawiak, E. Machaj, Z. Pojda, D. Wasilewska, J. Czubak, G. Hoser, Early severe impairment of hematopoietic stem and progenitor cells from the bone marrow caused by CLP sepsis and endotoxemia in a humanized mice model. *Stem Cell Res. Ther.* **6**, 142 (2015).

49. S. Rahmig, R. Kronstein-Wiedemann, J. Fohgrub, N. Kronstein, A. Nevmerzhitskaya, M. Bornhäuser, M. Gassmann, A. Platz, R. Ordemann, T. Tonn, C. Waskow, Improved Human Erythropoiesis and Platelet Formation in Humanized NSGW41 Mice. *Stem Cell Reports*. **7**, 591–601 (2016).

50. S. Belluschi, E. F. Calderbank, V. Ciaurro, B. Pijuan-Sala, A. Santoro, N. Mende, E. Diamanti, K. Y. C. Sham, X. Wang, W. W. Y. Lau, W. Jawaid, B. Göttgens, E. Laurenti, Myelo-lymphoid lineage restriction occurs in the human haematopoietic stem cell compartment before lymphoid-primed multipotent progenitors. *Nat. Commun.* **9**, 4100 (2018).

51. C. X. Wang, L. Zhang, B. Wang, One Cell At a Time (OCAT): a unified framework to integrate and analyze single-cell RNA-seq data. *Genome Biol.* **23**, 102 (2022).

52. G. W. Schwartz, Y. Zhou, J. Petrovic, M. Fasolino, L. Xu, S. M. Shaffer, W. S. Pear, G. Vahedi, R. B. Faryabi, TooManyCells identifies and visualizes relationships of single-cell clades. *Nat. Methods*. **17**, 405–413 (2020).

53. G. W. Schwartz, Y. Zhou, J. Petrovic, W. S. Pear, R. B. Faryabi, TooManyPeaks identifies drug-resistant-specific regulatory elements from single-cell leukemic epigenomes. *Cell Rep.* **36**, 109575 (2021).

54. M. A. Skinnider, J. W. Squair, C. Kathe, M. A. Anderson, M. Gautier, K. J. E. Matson, M. Milano, T. H. Hutson, Q. Barraud, A. A. Phillips, L. J. Foster, G. La Manno, A. J. Levine, G. Courtine, Cell type prioritization in single-cell data. *Nat. Biotechnol.* **39**, 30–34 (2021).

55. C. Bravo González-Blas, S. De Winter, G. Hulselmans, N. Hecker, I. Matetovici, V. Christiaens, S. Poovathingal, J. Wouters, S. Aibar, S. Aerts, SCENIC+: single-cell multiomic inference of enhancers and gene regulatory networks. *Nat. Methods*. **20**, 1355–1367 (2023).

56. S. Naik, S. B. Larsen, N. C. Gomez, K. Alaverdyan, A. Sendoel, S. Yuan, L. Polak, A.

Kulukian, S. Chai, E. Fuchs, Inflammatory memory sensitizes skin epithelial stem cells to tissue damage. *Nature*. **550**, 475–480 (2017).

57. S. Naik, E. Fuchs, Inflammatory memory and tissue adaptation in sickness and in health. *Nature*. **607**, 249–255 (2022).

58. S. B. Larsen, C. J. Cowley, S. M. Sajjath, D. Barrows, Y. Yang, T. S. Carroll, E. Fuchs, Establishment, maintenance, and recall of inflammatory memory. *Cell Stem Cell*. **28**, 1758–1774.e8 (2021).

59. D. L. Farber, N. A. Yudanin, N. P. Restifo, Human memory T cells: generation, compartmentalization and homeostasis. *Nat. Rev. Immunol.* **14**, 24–35 (2014).

60. R. S. Akondy, M. Fitch, S. Edupuganti, S. Yang, H. T. Kissick, K. W. Li, B. A. Youngblood, H. A. Abdelsamed, D. J. McGuire, K. W. Cohen, G. Alexe, S. Nagar, M. M. McCausland, S. Gupta, P. Tata, W. N. Haining, M. J. McElrath, D. Zhang, B. Hu, W. J. Greenleaf, J. J. Goronzy, M. J. Mulligan, M. Hellerstein, R. Ahmed, Origin and differentiation of human memory CD8 T cells after vaccination. *Nature*. **552**, 362–367 (2017).

61. A. M. Intlekofer, N. Takemoto, E. J. Wherry, S. A. Longworth, J. T. Northrup, V. R. Palanivel, A. C. Mullen, C. R. Gasink, S. M. Kaech, J. D. Miller, L. Gapin, K. Ryan, A. P. Russ, T. Lindsten, J. S. Orange, A. W. Goldrath, R. Ahmed, S. L. Reiner, Effector and memory CD8+ T cell fate coupled by T-bet and eomesodermin. *Nat. Immunol.* **6**, 1236–1244 (2005).

62. J.-G. Cheong, A. Ravishankar, S. Sharma, C. N. Parkhurst, S. A. Grassmann, C. K. Wingert, P. Laurent, S. Ma, L. Paddock, I. C. Miranda, E. O. Karakaslar, D. Nehar-Belaid, A. Thibodeau, M. J. Bale, V. K. Kartha, J. K. Yee, M. Y. Mays, C. Jiang, A. W. Daman, A. Martinez de Paz, D. Ahimovic, V. Ramos, A. Lercher, E. Nielsen, S. Alvarez-Mulett, L. Zheng, A. Earl, A. Yallowitz, L. Robbins, E. LaFond, K. L. Weidman, S. Racine-Brzostek, H. S. Yang, D. R. Price, L. Leyre, A. F. Rendeiro, H. Ravichandran, J. Kim, A. C. Borczuk, C. M. Rice, R. B. Jones, E. J. Schenck, R. J. Kaner, A. Chadburn, Z. Zhao, V. Pascual, O. Elemento, R. E. Schwartz, J. D. Buenrostro, R. E. Niec, F. J. Barrat, L. Lief, J. C. Sun, D. Ucar, S. Z. Josefowicz, Epigenetic memory of coronavirus infection in innate immune cells and their progenitors. *Cell*. **186**, 3882–3902.e24 (2023).

63. C. Franceschi, P. Garagnani, P. Parini, C. Giuliani, A. Santoro, Inflammaging: a new immune-metabolic viewpoint for age-related diseases. *Nat. Rev. Endocrinol.* **14**, 576–590 (2018).

64. N. A. Jakobsen, S. Turkalj, A. Zeng, B. Stoilova, M. Metzner, M. S. Nagree, S. Shah, R. Moore, B. Usukhbayar, M. A. Salazar, G.-A. Gafencu, A. Kennedy, S. Newman, B. J. L. Kendrick, A. H. Taylor, R. Afinowi-Luitz, R. Gundle, B. Watkins, K. Wheway, D. Beazley, A. Murison, A. G. Aguilar-Navarro, E. Flores-Figueroa, S. G. Dakin, A. J. Carr, C. Nerlov, J. E. Dick, S. Z. Xie, P. Vyas, Selective advantage of mutant stem cells in clonal hematopoiesis occurs by attenuating the deleterious effects of inflammation and aging. *Cell Stem Cell*.

65. M. Ainciburu, T. Ezponda, N. Berastegui, A. Alfonso-Pierola, A. Vilas-Zornoza, P. San Martin-Uriz, D. Alignani, J. Lamo-Espinosa, M. San-Julian, T. Jiménez-Solas, F. Lopez, S. Muntion, F. Sanchez-Guijo, A. Molero, J. Montoro, G. Serrano, A. Diaz-Mazkiaran, M. Lasaga, D. Gomez-Cabrero, M. Diez-Campelo, D. Valcarcel, M. Hernaez, J. P. Romero, F. Prosper, Uncovering perturbations in human hematopoiesis associated with healthy aging

and myeloid malignancies at single-cell resolution. *Elife*. **12** (2023), doi:10.7554/eLife.79363.

66. Y. Zhang, X. Xie, Y. Huang, M. Liu, Q. Li, J. Luo, Y. He, X. Yin, S. Ma, W. Cao, S. Chen, J. Peng, J. Guo, W. Zhou, H. Luo, F. Dong, H. Cheng, S. Hao, L. Hu, P. Zhu, T. Cheng, Temporal molecular program of human hematopoietic stem and progenitor cells after birth. *Dev. Cell*. **57**, 2745–2760.e6 (2022).

67. K. A. Oetjen, K. E. Lindblad, M. Goswami, G. Gui, P. K. Dagur, C. Lai, L. W. Dillon, J. P. McCoy, C. S. Hourigan, Human bone marrow assessment by single-cell RNA sequencing, mass cytometry, and flow cytometry. *JCI Insight*. **3** (2018), doi:10.1172/jci.insight.124928.

68. M. Setty, V. Kiseliovas, J. Levine, A. Gayoso, L. Mazutis, D. Pe'er, Characterization of cell fate probabilities in single-cell data with Palantir. *Nat. Biotechnol.* **37**, 451–460 (2019).

69. N. Mende, H. P. Bastos, A. Santoro, K. T. Mahbubani, V. Ciaurro, E. F. Calderbank, M. Quiroga Londoño, K. Sham, G. Mantica, T. Morishima, E. Mitchell, M. R. Lidonnici, F. Meier-Abt, D. Hayler, L. Jardine, A. Curd, M. Haniffa, G. Ferrari, H. Takizawa, N. K. Wilson, B. Göttgens, K. Saeb-Parsy, M. Frontini, E. Laurenti, Unique molecular and functional features of extramedullary hematopoietic stem and progenitor cell reservoirs in humans. *Blood*. **139**, 3387–3401 (2022).

70. A. Regev, S. A. Teichmann, E. S. Lander, I. Amit, C. Benoist, E. Birney, B. Bodenmiller, P. Campbell, P. Carninci, M. Clatworthy, H. Clevers, B. Deplancke, I. Dunham, J. Eberwine, R. Eils, W. Enard, A. Farmer, L. Fugger, B. Göttgens, N. Hacohen, M. Haniffa, M. Hemberg, S. Kim, P. Klenerman, A. Kriegstein, E. Lein, S. Linnarsson, E. Lundberg, J. Lundeberg, P. Majumder, J. C. Marioni, M. Merad, M. Mhlanga, M. Nawijn, M. Netea, G. Nolan, D. Pe'er, A. Phillipakis, C. P. Ponting, S. Quake, W. Reik, O. Rozenblatt-Rosen, J. Sanes, R. Satija, T. N. Schumacher, A. Shalek, E. Shapiro, P. Sharma, J. W. Shin, O. Stegle, M. Stratton, M. J. T. Stubbington, F. J. Theis, M. Uhlen, A. van Oudenaarden, A. Wagner, F. Watt, J. Weissman, B. Wold, R. Xavier, N. Yosef, Human Cell Atlas Meeting Participants, The Human Cell Atlas. *Elife*. **6** (2017), doi:10.7554/eLife.27041.

71. S. Jaiswal, P. Fontanillas, J. Flannick, A. Manning, P. V. Grauman, B. G. Mar, R. C. Lindsley, C. H. Mermel, N. Burtt, A. Chavez, J. M. Higgins, V. Moltchanov, F. C. Kuo, M. J. Kluk, B. Henderson, L. Kinnunen, H. A. Koistinen, C. Ladenvall, G. Getz, A. Correa, B. F. Banahan, S. Gabriel, S. Kathiresan, H. M. Stringham, M. I. McCarthy, M. Boehnke, J. Tuomilehto, C. Haiman, L. Groop, G. Atzmon, J. G. Wilson, D. Neuberg, D. Altshuler, B. L. Ebert, Age-related clonal hematopoiesis associated with adverse outcomes. *N. Engl. J. Med.* **371**, 2488–2498 (2014).

72. G. Genovese, A. K. Kähler, R. E. Handsaker, J. Lindberg, S. A. Rose, S. F. Bakhoum, K. Chambert, E. Mick, B. M. Neale, M. Fromer, S. M. Purcell, O. Svantesson, M. Landén, M. Höglund, S. Lehmann, S. B. Gabriel, J. L. Moran, E. S. Lander, P. F. Sullivan, P. Sklar, H. Grönberg, C. M. Hultman, S. A. McCarroll, Clonal hematopoiesis and blood-cancer risk inferred from blood DNA sequence. *N. Engl. J. Med.* **371**, 2477–2487 (2014).

73. F. Notta, S. Doulatov, E. Laurenti, A. Poeppl, I. Jurisica, J. E. Dick, Isolation of single human hematopoietic stem cells capable of long-term multilineage engraftment. *Science*. **333**, 218–221 (2011).

74. W. J. Wong, C. Emdin, A. G. Bick, S. M. Zekavat, A. Niroula, J. P. Pirruccello, L. Dichtel, G.

Griffin, M. M. Uddin, C. J. Gibson, V. Kovalcik, A. E. Lin, M. E. McConkey, A. Vromman, R. S. Sellar, P. G. Kim, M. Agrawal, J. Weinstock, M. T. Long, B. Yu, R. Banerjee, R. C. Nicholls, A. Dennis, M. Kelly, P.-R. Loh, S. McCarroll, E. Boerwinkle, R. S. Vasan, S. Jaiswal, A. D. Johnson, R. T. Chung, K. Corey, D. Levy, C. Ballantyne, NHLBI TOPMed Hematology Working Group, B. L. Ebert, P. Natarajan, Clonal haematopoiesis and risk of chronic liver disease. *Nature*. **616**, 747–754 (2023).

75. S. Jaiswal, P. Natarajan, A. J. Silver, C. J. Gibson, A. G. Bick, E. Shvartz, M. McConkey, N. Gupta, S. Gabriel, D. Ardissino, U. Baber, R. Mehran, V. Fuster, J. Danesh, P. Frossard, D. Saleheen, O. Melander, G. K. Sukhova, D. Neuberg, P. Libby, S. Kathiresan, B. L. Ebert, Clonal Hematopoiesis and Risk of Atherosclerotic Cardiovascular Disease. *N. Engl. J. Med.* **377**, 111–121 (2017).

76. M. Xie, C. Lu, J. Wang, M. D. McLellan, K. J. Johnson, M. C. Wendl, J. F. McMichael, H. K. Schmidt, V. Yellapantula, C. A. Miller, B. A. Ozenberger, J. S. Welch, D. C. Link, M. J. Walter, E. R. Mardis, J. F. Dipersio, F. Chen, R. K. Wilson, T. J. Ley, L. Ding, Age-related mutations associated with clonal hematopoietic expansion and malignancies. *Nat. Med.* **20**, 1472–1478 (2014).

77. M. Greaves, A causal mechanism for childhood acute lymphoblastic leukaemia. *Nat. Rev. Cancer*. **18**, 471–484 (2018).

78. B. S. McEwen, Interacting mediators of allostasis and allostatic load: towards an understanding of resilience in aging. *Metabolism*. **52**, 10–16 (2003).

79. P. van Galen, A. Kreso, N. Mbong, D. G. Kent, T. Fitzmaurice, J. E. Chambers, S. Xie, E. Laurenti, K. Hermans, K. Eppert, S. J. Marciniak, J. C. Goodall, A. R. Green, B. G. Wouters, E. Wienholds, J. E. Dick, The unfolded protein response governs integrity of the haematopoietic stem-cell pool during stress. *Nature*. **510**, 268–272 (2014).

80. M. Milyavsky, O. I. Gan, M. Trottier, M. Komosa, O. Tabach, F. Notta, E. Lechman, K. G. Hermans, K. Eppert, Z. Konovalova, O. Ornatsky, E. Domany, M. S. Meyn, J. E. Dick, A distinctive DNA damage response in human hematopoietic stem cells reveals an apoptosis-independent role for p53 in self-renewal. *Cell Stem Cell*. **7**, 186–197 (2010).

81. S. Ukraintseva, K. Arbeev, M. Duan, I. Akushevich, A. Kulminski, E. Stallard, A. Yashin, Decline in biological resilience as key manifestation of aging: Potential mechanisms and role in health and longevity. *Mech. Ageing Dev.* **194**, 111418 (2021).

82. M. Fiumara, S. Ferrari, A. Omer-Javed, S. Beretta, L. Albano, D. Canarutto, A. Varesi, C. Gaddoni, C. Brombin, F. Cugnata, E. Zonari, M. M. Naldini, M. Barcella, B. Gentner, I. Merelli, L. Naldini, Genotoxic effects of base and prime editing in human hematopoietic stem cells. *Nat. Biotechnol.* (2023), doi:10.1038/s41587-023-01915-4.

83. E. Wagenblast, M. Azkanaz, S. A. Smith, L. Shakib, J. L. McLeod, G. Krivdova, J. Araújo, L. D. Shultz, O. I. Gan, J. E. Dick, E. R. Lechman, Functional profiling of single CRISPR/Cas9-edited human long-term hematopoietic stem cells. *Nat. Commun.* **10**, 4730 (2019).

84. Y. Hu, G. K. Smyth, ELDA: extreme limiting dilution analysis for comparing depleted and enriched populations in stem cell and other assays. *J. Immunol. Methods*. **347**, 70–78 (2009).

85. M. S. Nagree, T. C. Felizardo, M. L. Faber, J. Rybova, C. A. Rupar, S. R. Foley, M. Fuller, D. H. Fowler, J. A. Medin, Autologous, lentivirus-modified, T-rapa cell “micropharmacies” for lysosomal storage disorders. *EMBO Mol. Med.* **14**, e14297 (2022).

86. D. T. Mulder, E. R. Mahé, M. Dowar, Y. Hanna, T. Li, L. T. Nguyen, M. O. Butler, N. Hirano, J. Delabie, P. S. Ohashi, T. J. Pugh, CapTCR-seq: hybrid capture for T-cell receptor repertoire profiling. *Blood Adv*. **2**, 3506–3514 (2018).

87. A. E. Magurran, Measuring biological diversity. *Curr. Biol.* **31**, R1174–R1177 (2021).

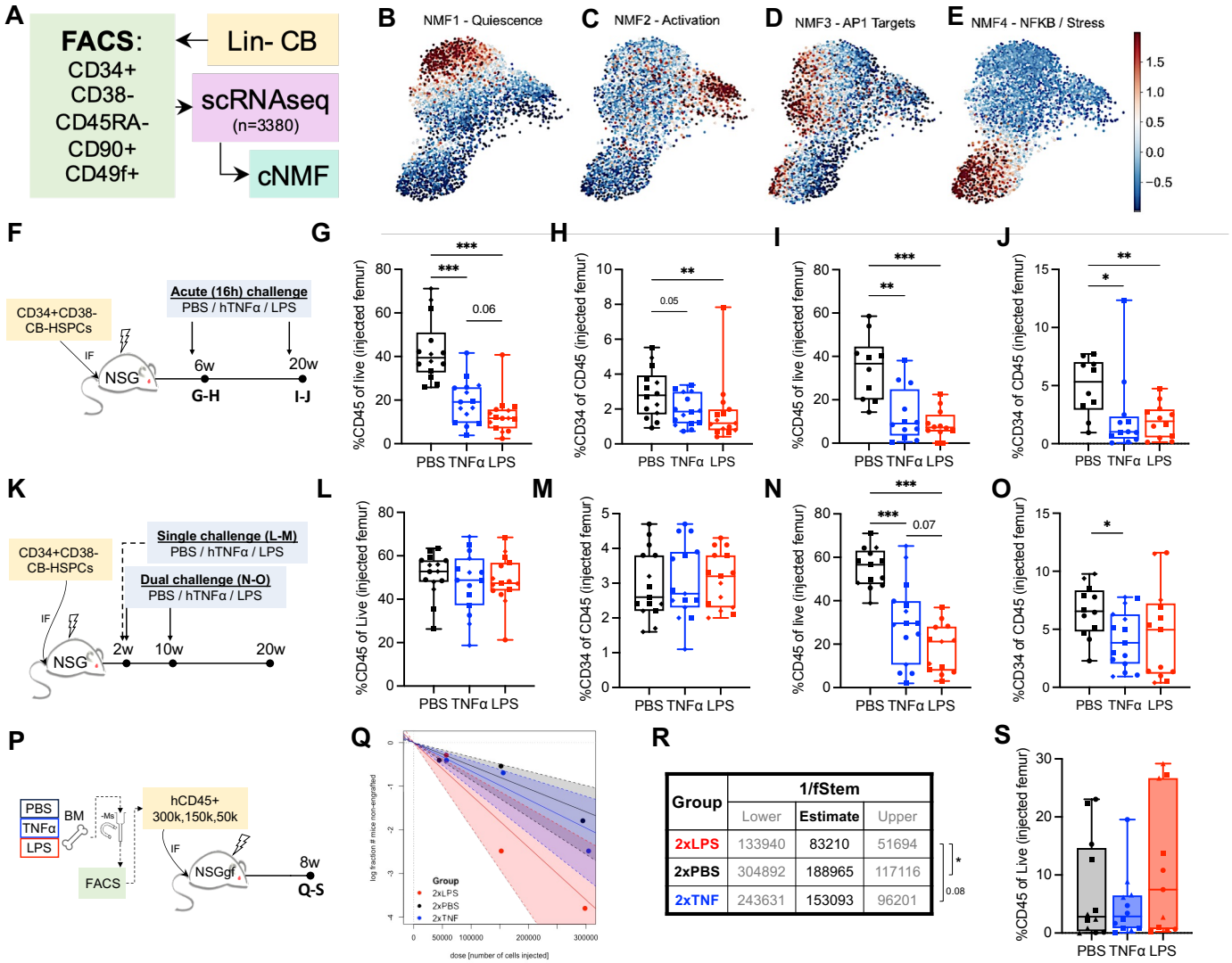

Group	1/fStem		
	Lower	Estimate	Upper
2xLPS	133940	83210	51694
2xPBS	304892	188965	117116
2xTNF	243631	153093	96201

Figure 1: Modeling inflammatory response and recovery in human LT-HSC. (**A**) Umbilical cord blood (CB) from multiple, mixed-sex donors were sorted for the indicated immunophenotype to purify LT-HSC. Cells were subjected to single cell (sc) RNA sequencing on the BD Rhapsody platform. Consensus non-negative matrix factorization (cNMF) was performed on the 3,380 cells that passed quality control (QC). (**B-E**) Localized enrichment of the cNMF transcriptional programs identified in (A), namely programs associated with quiescence (B), activation (C), and AP1-mediated (D) or NFkB-driven (E) transcription. (**F**) NSG mice xenografted with CB-derived CD34+CD38- cells via intrafemoral (IF) injection after irradiation were challenged with human tumor necrosis factor (hTNF)α or lipopolysaccharide (LPS) at either 6 weeks (G-H) or 20 weeks (I-J) post-engraftment. The effect on total human engraftment (G, I) and progenitor compartment (H,J) 16 hours after inflammatory challenge was measured and compared to mice challenged with vehicle control (PBS). (**K**) Schematic for xenograft model of recovery from single (2 weeks) or dual (2 weeks and 10 weeks) acute inflammatory challenge. (**L-M**) Human engraftment (L) and progenitor composition (M) 18 weeks after a single inflammatory challenge. (**N-O**) Human engraftment (N) and progenitor composition (O) 10 weeks after dual inflammatory challenge. (**P**) Experimental schematic for secondary transplantation. Bone marrow from dual-challenged mice as in (K) was depleted for murine cells and subjected to fluorescence-activated cell sorting (FACS) for human leukocytes. Secondary transplantation with limiting dilution was performed with the indicated cell doses in NSG-SGM3 (growth factor mice; gf) and engraftment evaluated after 8 weeks. (**Q-R**) Stem cell frequency estimates calculated for secondary transplants in (P). (**S**) Proportion of engrafted human cells in cohorts from (P) transplanted with 300,000 hCD45+ cells. All engraftment data is presented as box plots with a line at the median, boxes showing quartiles and error bars showing range. Individual points show data for each animal used in the study (n=10-15), and different symbols reflect different CB pools (n=2-3). Data were compared using pairwise Mann-Whitney tests; *** p<0.001, ** p<0.01, * p<0.05, and p<0.1 is shown numerically, while p>0.1 is not shown. Stem cell frequency estimates were compared using chi-squared tests, * p<0.05, and p<0.1 is shown numerically, while p>0.1 is not shown.

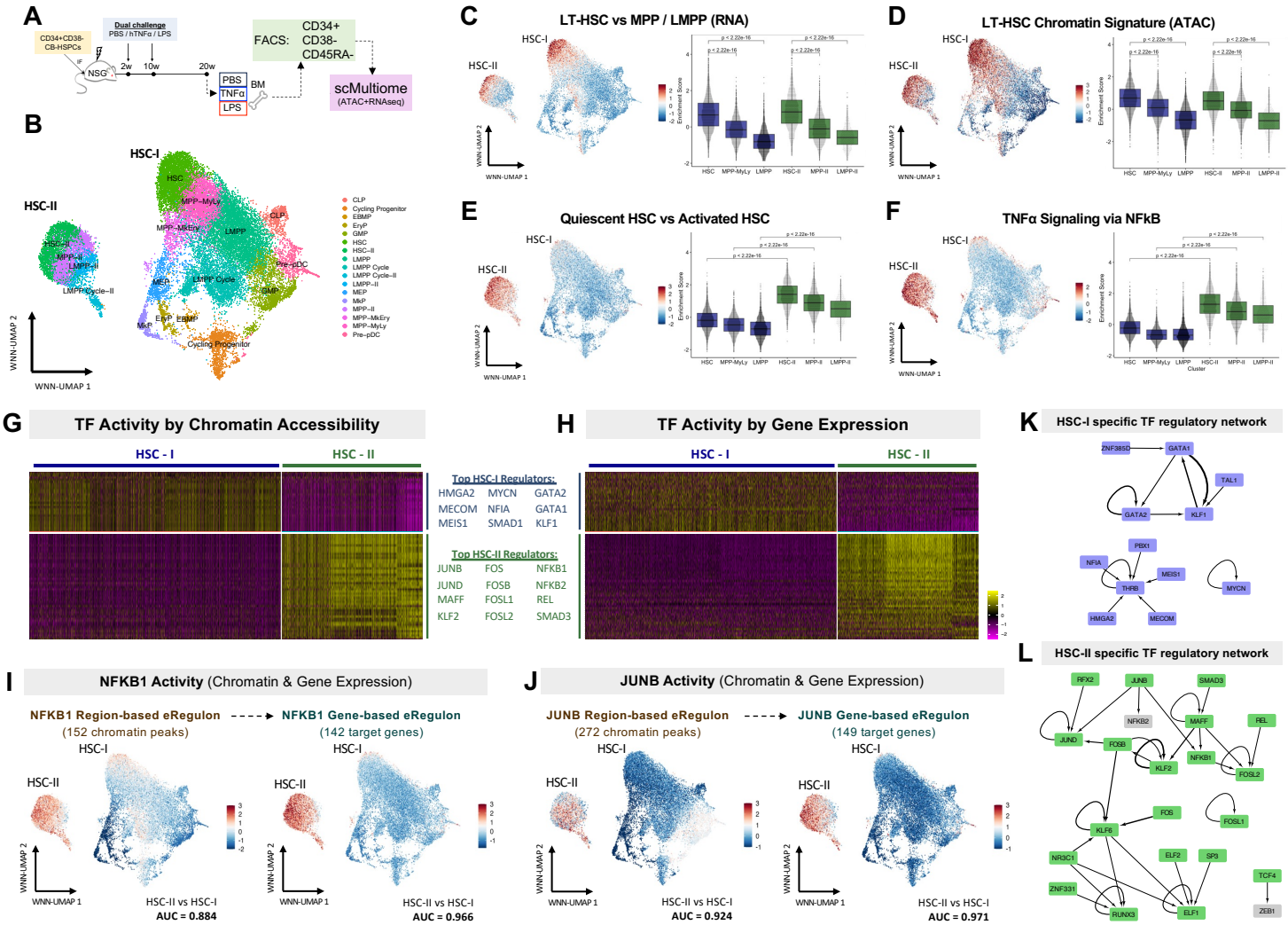

Figure 2: Two human HSC populations identified in an inflammatory recovery model. **A**) Schematic outlining Multiome profiling of xenografted Prim (CD45+CD34+CD38-CD45RA-) CB-derived HSPCs following dual *in vivo* inflammatory challenge and subsequent recovery with either PBS, TNFα, or LPS. **B**) UMAP of 27,492 xenografted HSPCs based on integrated RNA and ATAC embeddings from weighted nearest-neighbour (WNN) analysis. **C-F**) Normalized signature enrichment scores (AUCell), overlaid on the WNN UMAP embedding and depicted as boxplots for HSC, MPP, LMPP, and HSC-II, MPP-II, LMPP-II populations. Statistical comparisons are made with a Wilcoxon rank sum test. **C**) Enrichment of an LT-HSC-specific gene signature from sorted fraction bulk RNA-seq in CB. **D**) Enrichment of an LT-HSC-specific chromatin accessibility signature from sorted fraction bulk ATAC-seq in CB. **E**) Enrichment of a gene expression signature specific to uncultured, quiescent, CB LT-HSC relative to CB LT-HSC activated from 96hr in *in vitro* culture. **F**) Enrichment of hallmark geneset corresponding to TNFα signaling via NF-kB. **G-H**) Enrichment of TF activity in either HSC-I or HSC-II based on target chromatin region accessibility **G**) and target gene expression **H**) inferred through SCENIC+. Each row in heatmap (G) corresponds to the same TF as the equivalent row in heatmap (H). Top regulators for each cell state are also written as shown. **I-J**) SCENIC+ inferred TF activity of HSC-II specific TFs NFKB1 (I) and JUNB (J) on the basis of target chromatin peak accessibility and expression of target genes regulated by these target chromatin peaks. AUC scores for discriminatory power between HSC-I and HSC-II are also depicted for each TF activity estimate. **K-L**) TF regulatory networks specific to either HSC-I (K) or HSC-II (L) from SCENIC+. TFs with significant enrichment in both gene expression activity and chromatin accessibility activity in either HSC-I or HSC-II are colored in blue or green, respectively. Regulation strength between TFs, based on both chromatin accessibility and gene expression, is represented through edge width in the graph.

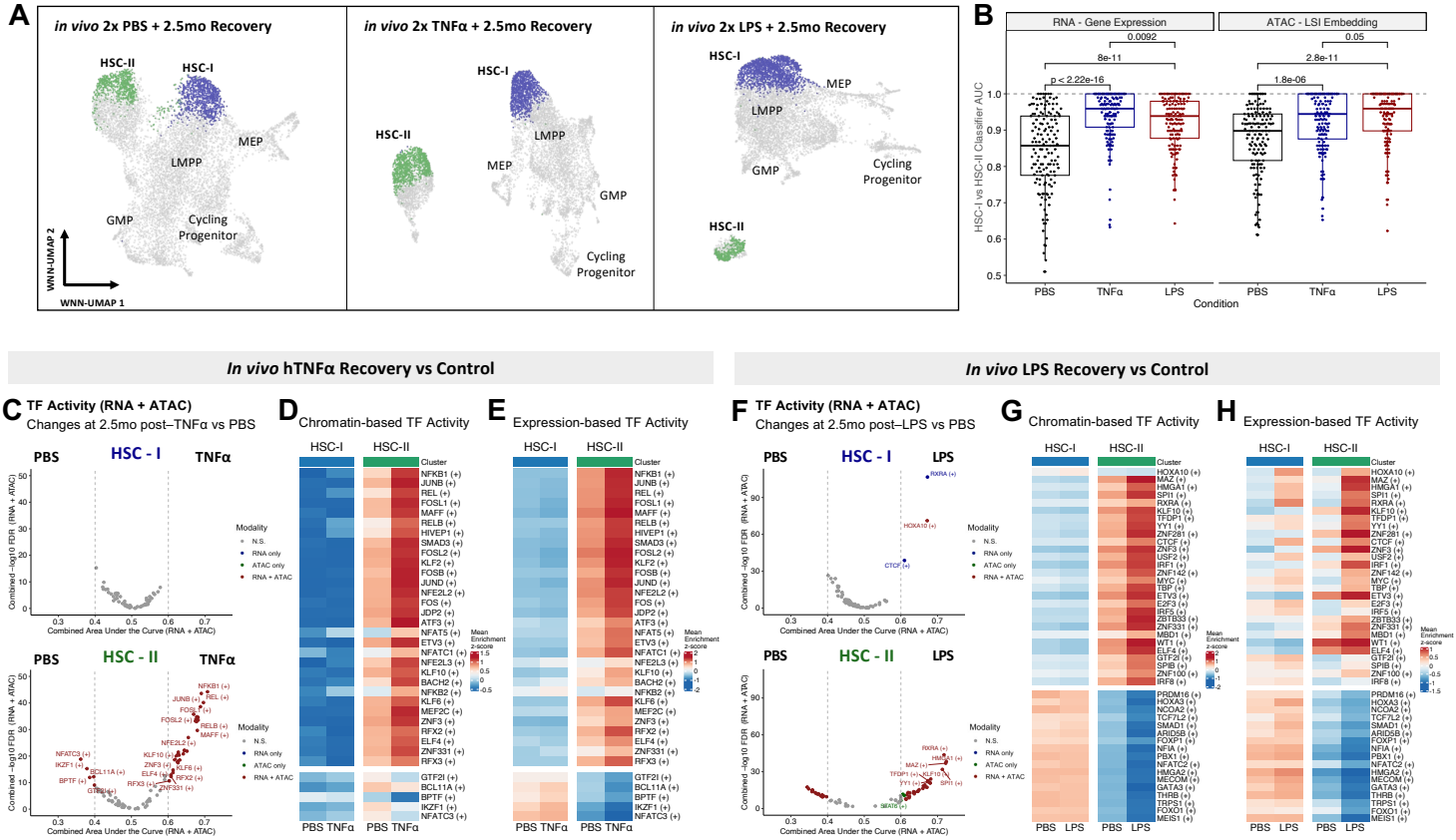

Figure 3: HSC-II retains memory of prior inflammatory stress. **A**) Combined RNA + ATAC WNN UMAP of xenografted Prim CB-derived HSPCs, split by treatment condition into *in vivo* dual PBS challenge + 10w recovery (n = 9,756), *in vivo* dual TNFα challenge + 10w recovery (n = 8,785), or *in vivo* dual LPS challenge + 10w recovery (n = 8,951). **B**) Separability of HSC-I and HSC-II on the basis of gene expression (expression highly variable genes) and chromatin accessibility (50 LSI components) within each experimental condition. Each point represents the AUC of a random forest classifier trained to predict HSC-I vs HSC-II status from 150 subsamples of the data using Augur. **C-E**) Differential SCENIC+ TF activity between *in vivo* dual TNFα challenge + 10w recovery compared to PBS control, stratified by HSC subset. **C**) Volcano plot of differentially enriched TFs between TNFα and PBS conditions. Y-axis portrays the combined significance level of differential enrichment by a linear mixed model accounting for donor sex. X-axis portrays the combined AUC statistic for discerning between TNFα and PBS conditions. AUC and significance metrics are calculated independently for RNA-based TF activity and ATAC-based TF activity, with the mean value between the two modalities representing the combined metric. TFs are colored based on significance at FDR < 0.05 and either AUC < 0.4 or AUC > 0.6. TFs that meet criteria for both RNA and ATAC are colored red. **D**) Chromatin-based TF activity of differentially enriched TFs between TNFα and PBS conditions. Mean enrichment score is depicted for each condition and each HSC subset. **E**) Expression-based TF activity of differentially enriched TFs between TNFα and PBS conditions. Mean enrichment score is depicted for each condition and each HSC subset. **F-H**) Differential SCENIC+ TF activity between *in vivo* dual LPS challenge + 10w recovery compared to PBS control, stratified by HSC subset. **F**) Volcano plot of differentially enriched TFs between LPS and PBS conditions. **D**) Chromatin-based TF activity of differentially enriched TFs between TNFα and PBS conditions. Mean enrichment score is depicted for each condition and each HSC subset. **E**) Expression-based TF activity of differentially enriched TFs between TNFα and PBS conditions. Mean enrichment score is depicted for each condition and each HSC subset.

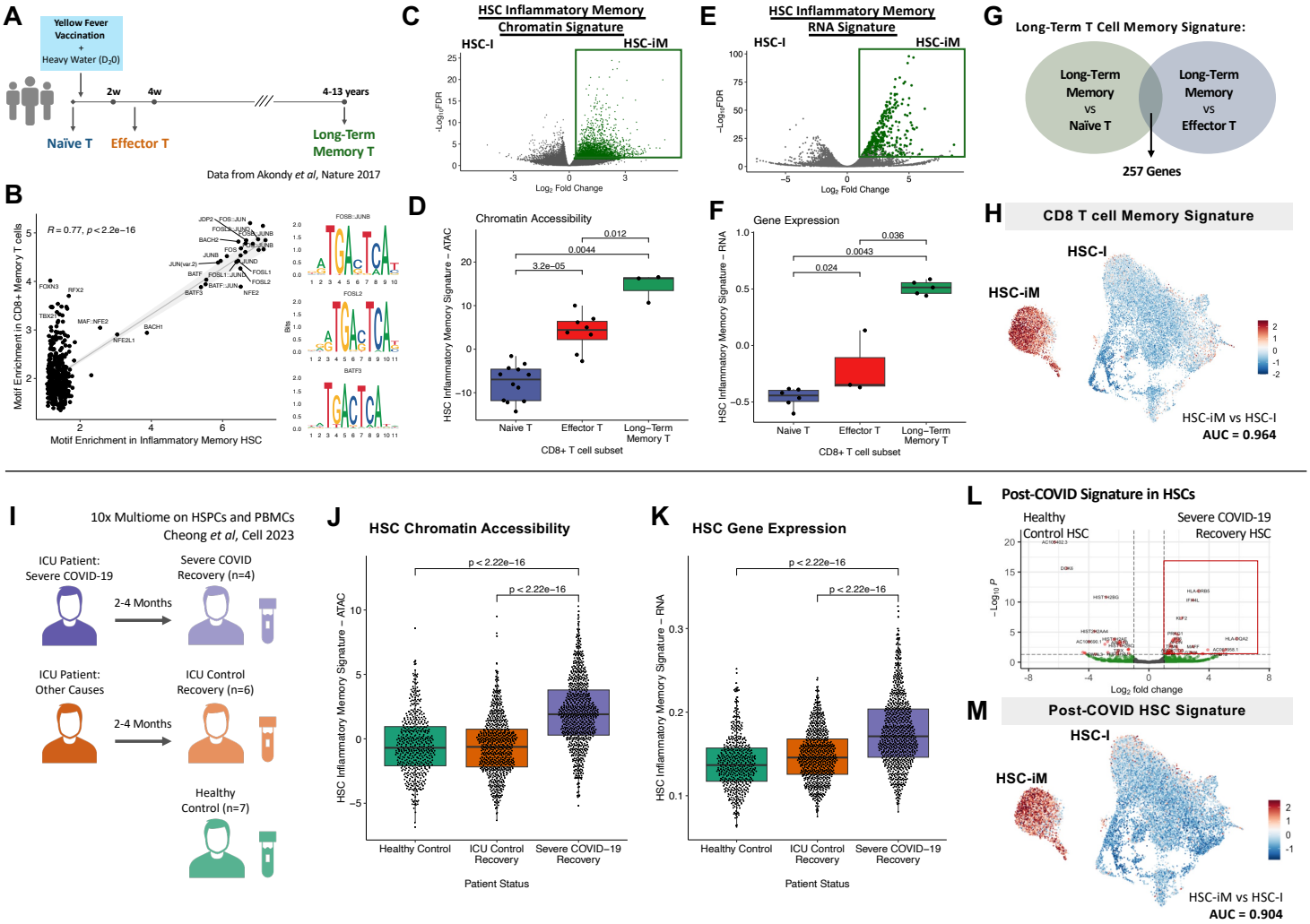

Figure 4: HSC inflammatory memory resembles human T cell memory and is induced by COVID-19 infection.
A) Schematic outlining purification of Naïve, Effector, and Long-Term Memory CD8 T cells from human volunteers from Akondy *et al*. These populations were profiled by bulk RNA-seq and ATAC-seq. **B**) TF motif enrichment analysis (fold enrichment) among differentially accessible regions (DARs) specific to memory T cells and DARs specific to inflammatory memory HSCs, quantified through Pearson correlation analysis. Three co-enriched motifs between inflammatory memory HSCs and memory T cells are shown as examples. **C**) 3,663 DARs specific to HSC-iM (vs HSC-I) constituting an epigenetic inflammatory memory signature. **E**) Enrichment of chromatin accessibility-based HSC inflammatory memory signature within human T cell subsets. Statistical comparisons were made using Wilcoxon rank sum tests. **D**) Top 200 differentially expressed genes (DEGs) specific to HSC-iM (vs HSC-I) constituting an expression-based inflammatory memory signature. **F**) Enrichment of gene expression-based HSC inflammatory memory signature within human T cell subsets. **G**) Derivation of a human CD8 long-term T cell memory signature. 257 genes were significantly enriched (FDR < 0.01, LFC > 1) in Memory T cells compared to Naive T cells as well as in Memory T cells compared to Effector T cells. **H**) Scoring of the CD8 long-term T cell memory signature in xenograft Multiome data. AUC score for discriminatory power between HSC-I and HSC-II is also depicted for this T cell signature. **I**) Schematic outlining experimental setup of HSPC Multiome from donors 2-4 months following severe COVID-19 infection as well as ICU recovery controls and healthy controls from Cheong *et al*. **J**) Enrichment of HSC inflammatory memory signatures within human HSCs that had endured prior severed COVID-19 illness and ICU or healthy control HSCs, scored on the basis of chromatin accessibility (J) and gene expression (K). Statistical comparisons were made using Wilcoxon rank sum tests. **L**) Derivation of a post-COVID HSC signature. 49 genes were significantly enriched in (FDR < 0.05) in severe COVID-19 recovery HSCs compared to healthy HSCs. **M**) Scoring of the post-COVID HSC signature in xenograft Multiome data. AUC score for discriminatory power between HSC-I and HSC-II is also depicted.

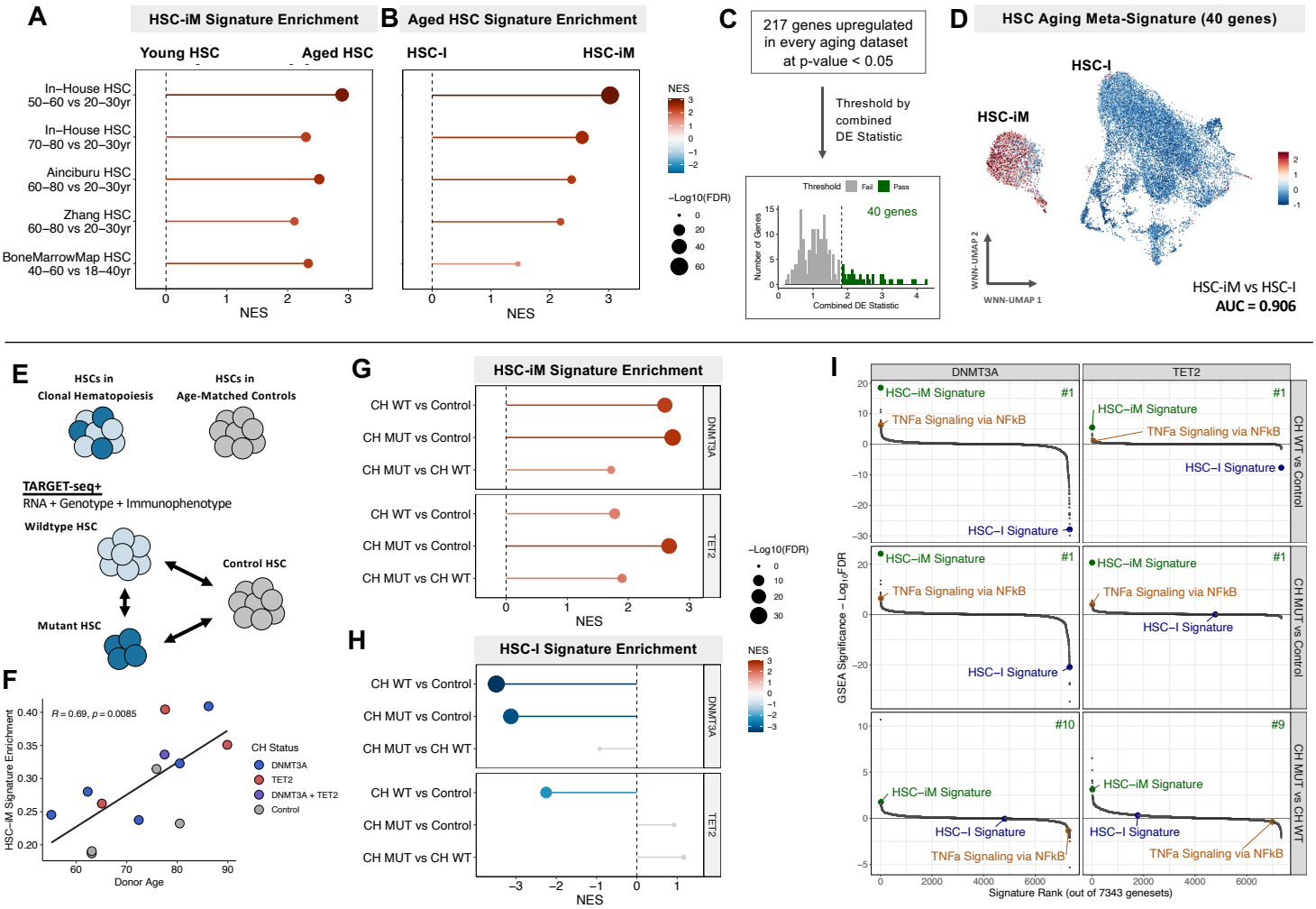

Figure 5: HSC inflammatory memory programs accumulate with human aging and CH.
A) GSEA results depicting HSC-iM gene expression signature enrichment in differential expression results between five separate comparisons of older aged (OA) and middle aged (MA) vs young adult (YA) human HSC, purified in silico through hematopoietic reference map projection. These include in-house data (two YA 20-30yr donors; two MA 50-60yr donors; two OA 70-80yr donors), Ainciburu et al (three OA 60-80yr donors; three YA 20-30yr donors), Zhang et al (three OA 60-80yr donors; two YA 20-30yr donors), and published datasets within our hematopoietic reference map (fourteen MA 40-60yr donors; nineteen YA 18-40yr donors). **B**) GSEA results depicting enrichment of Aged HSC signatures in HSC-iM and HSC-I, wherein significant DE genes specific to OA or MA HSC vs YA HSC from each dataset were evaluated by GSEA in differential expression results between HSC-iM and HSC-I from the xenograft Multiome data. **C**) Derivation of an Aged HSC-specific meta-signature from integrating results of the five human HSC aging comparisons in (B). Genes upregulated in OA or MA HSC vs YA HSC at uncorrected *P*-value < 0.05 in each of the five Aged vs Young HSC comparisons were retained, and the geometric mean of the DE test statistic from each of five comparisons was used to represent the combined DE statistic. After adaptive threshold, 40 genes remained that were significantly upregulated in HSC Aging from multiple independent datasets. **D**) Scoring of 40-gene Aged HSC meta-signature in xenograft Multiome data. AUC score for discriminatory power between HSC-I and HSC-II is also depicted. **E**) Schematic outlining TARGET-Seq+ profiling of HSPCs from 9 CH donors and 4 non-CH controls. Index-sorted HSCs and progenitors were profiled subject to single cell transcriptome profiling with concurrent genotyping of donor-specific CH driver mutations. **F)** Median HSC-iM gene expression signature enrichment of 4,951 transcriptional HSC/MPPs from CH and non-CH donors plotted against donor Age. Pearson correlation test results are depicted. **G-H**) GSEA results depicting HSC-iM (G) and HSC-I (H) gene expression signature enrichment in differential expression results between HSC/MPPs from conditions spanning Control, CH^{WT}, and CH^{MUT}, adjusting for donor ID, donor age, donor sex, and FACS sort as covariates. Positive enrichment indicates upregulation in CH while negative enrichment indicates downregulation in CH. Results are faceted by CH mutation type. **I**) Benchmarking of GSEA results from HSC-iM and HSC-I signatures against GSEA results from 7,341 additional pathways and genesets from MSigDB. The y axis depicts the absolute value of the $\log_{10}$(FDR) statistic from GSEA in the direction of the enrichment (positive for CH). The enrichment rank of the HSC-iM signature is depicted in the top right corner of each comparison. Results are faceted by CH mutation type.

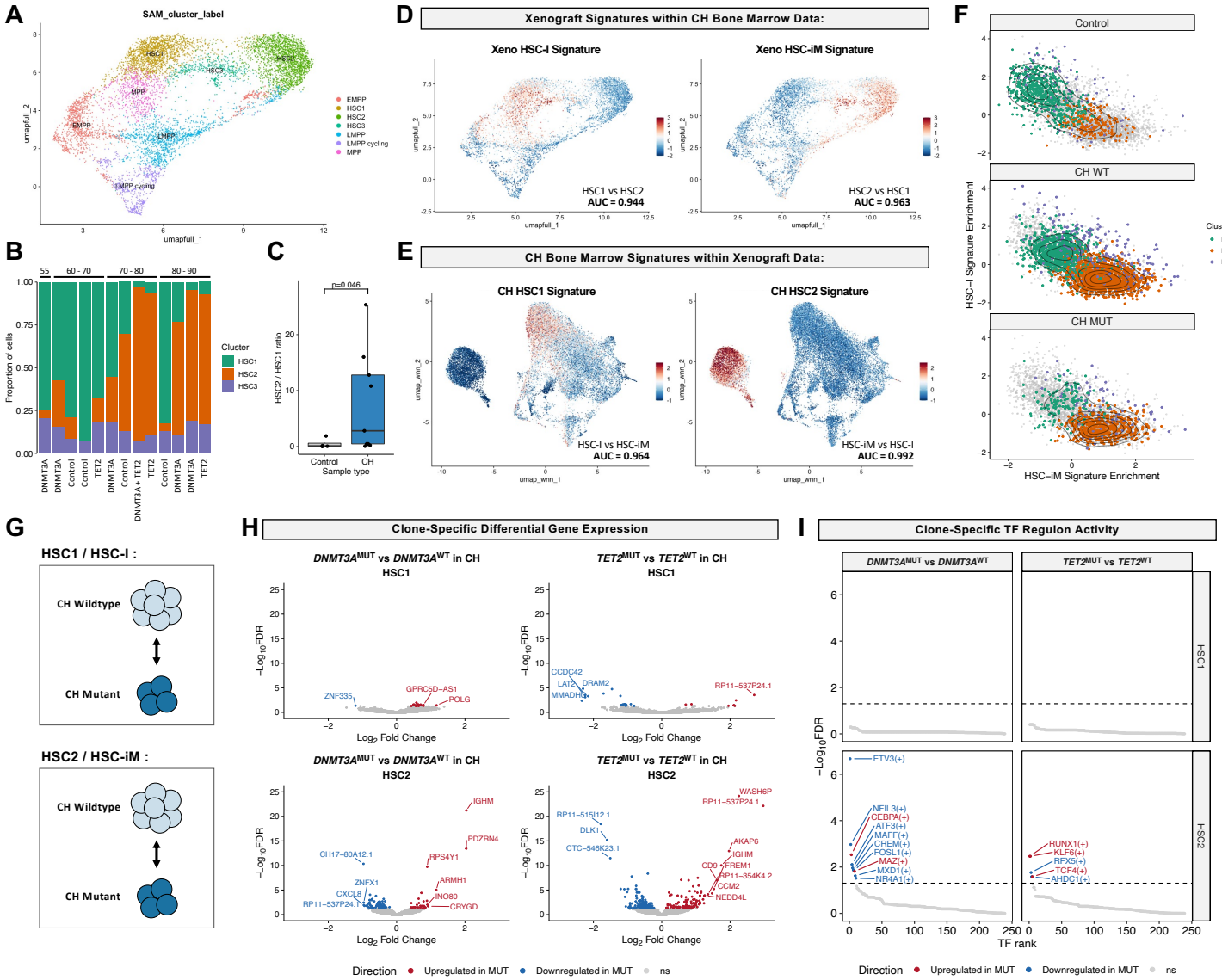

Figure 6: Clone-specific gene expression changes in CH are observed predominantly in HSC-iM.
A) UMAP of 8,059 bone marrow HSPCs from 9 donors with CH and 4 age-matched samples without CH, after unsupervised feature selection and clustering using the Self-Assembling Manifolds (SAM) algorithm. **B**) Proportion of cells in the HSC1, HSC2, and HSC3 clusters by donor. Donors are ordered by age and labelled according to their CH mutation status. Only cells sorted from the Lin$^-$CD34$^+$ FACS gate were included, excluding Lin$^-$CD34$^+$CD38$^-$ enriched cells. **C**) Ratio of HSC2 to HSC1 cells, comparing donors with CH and controls without CH. Only cells sorted from the Lin$^-$CD34$^+$ FACS gate were included, excluding Lin$^-$CD34$^+$CD38$^-$ enriched cells. Statistical comparison was made using a *t*-test. **D**) Scoring of the xenograft HSC-I and HSC inflammatory memory signatures in CH BM HSPC data. AUC score for discriminatory power between HSC1 and HSC2 is also depicted for these signatures. **E**) Scoring of the CH BM HSC1 and HSC2 cluster signatures in xenograft data. AUC score for discriminatory power between HSC-I and HSC-iM is also depicted. **F**) Enrichment of HSC-I and HSC-iM signatures in cells belonging to each of the three HSC clusters from Control and CH donors separated by genotype. **G**) Schematic showing the strategy for differential expression analysis between CH^{MUT} and CH^{WT} cells in either the HSC1 or HSC2 clusters. **H**) Volcano plot of differentially expressed genes between CH^{MUT} and CH^{WT} cells within the HSC1 and HSC2 clusters. Genes are colored based on significance at FDR < 0.05. **I**) Differential TF activity inferred by SCENIC between CH^{MUT} and CH^{WT} cells in either the HSC1 or HSC2 cluster. Y-axis portrays the significance level of differential enrichment by a linear mixed model accounting for donor identity. TFs are colored based on significance at FDR < 0.05.